CMS-BPH-12-006

arXiv:1501.07750v2 [hep-ex] 30 Jul 2015

Measurements of the Y(1S), Y(2S), and Y(3S) differential cross sections in pp collisions at $\sqrt{s} = 7\,\text{TeV}$

The CMS Collaboration[*]

Abstract

Differential cross sections as a function of transverse momentum p_T are presented for the production of Y(nS) ($n = 1, 2, 3$) states decaying into a pair of muons. Data corresponding to an integrated luminosity of $4.9\,\text{fb}^{-1}$ in pp collisions at $\sqrt{s} = 7\,\text{TeV}$ were collected with the CMS detector at the LHC. The analysis selects events with dimuon rapidity $|y| < 1.2$ and dimuon transverse momentum in the range $10 < p_T < 100\,\text{GeV}$. The measurements show a transition from an exponential to a power-law behavior at $p_T \approx 20\,\text{GeV}$ for the three Y states. Above that transition, the Y(3S) spectrum is significantly harder than that of the Y(1S). The ratios of the Y(3S) and Y(2S) differential cross sections to the Y(1S) cross section show a rise as p_T increases at low p_T, then become flatter at higher p_T.

[*]See Appendix B for the list of collaboration members

1 Introduction

Hadronic production of S-wave $b\bar{b}$ mesons has been extensively studied for many years. At the CERN LHC, the CMS [1, 2], ATLAS [3], and LHCb [4] Collaborations have published results on $Y(nS)$ (n = 1, 2, 3) production cross sections times dimuon branching fractions in pp collisions at $\sqrt{s} = 7$ TeV as a function of the Y transverse momentum p_T, rapidity y, and polarization [5]. The CMS and ATLAS p_T and $|y|$ distributions in the central rapidity region $|y| < 2.0$ are similar in shape to those from $p\bar{p}$ production at $\sqrt{s} = 1.96$ TeV, as measured by the D0 [6] and CDF [7] experiments at the Tevatron. Neither the ATLAS nor the CMS results show any statistically significant rapidity dependence of the cross section in the central region. The CMS analyses cover the p_T range up to 50 GeV, while the ATLAS results go to 70 GeV.

In this Letter we present a measurement of the differential production cross sections of the three lowest-mass $Y(nS)$ states in pp collisions at $\sqrt{s} = 7$ TeV up to $p_T = 100$ GeV, reaching higher p_T than previous measurements. We measure the p_T dependence of the $Y(nS)$ differential cross section times the branching fraction to $\mu^+\mu^-$ using the 2011 data set, corresponding to an integrated luminosity of 4.9 fb^{-1}. The measured cross sections include feeddown from higher $b\bar{b}$ excitations.

Measurements of S-wave $b\bar{b}$ mesons provide an important probe of quantum chromodynamics (QCD). There are several models that predict differential cross section shapes at high $Y(nS)$ p_T in pp collisions. A common feature of all the models is that different contributing terms have different p_T variations, some of which are power-law forms. The nonrelativistic QCD (NRQCD) approach [8, 9] uses an effective field theory to factorize the perturbative term and nonperturbative long-distance matrix element (LDME) terms. A good description of early LHC results for $Y(1S)$ production for $p_T < 30$ GeV was achieved using NRQCD with next-to-leading-order (NLO) corrections [10]. However, there are theoretical corrections to perturbative NRQCD that have characteristic power-law behavior at high p_T, and measurements at high p_T can help to clarify the theoretical picture [11, 12]. The NLO NRQCD calculation has recently been extended to treat all three $Y(nS)$ states [13]. The updated calculation includes not only NLO terms but also uses LDMEs computed using only high-p_T data. Color singlet models (CSM) with higher-order p_T-dependent corrections [14] and the k_T-factorization model [15] are consistent with data from the LHC for p_T approaching 50 GeV. A recent analysis of quarkonium polarization and production measurements found that raising p_T thresholds stabilizes the fits in evaluating the LDMEs [16]. At higher p_T different corrections become dominant in these models. New data at high p_T will challenge all the current approaches.

2 CMS detector

The central feature of the CMS apparatus is a superconducting solenoid of 6 m internal diameter having a 3.8 T field. Within the superconducting solenoid volume are a silicon pixel and strip tracker, a lead tungstate crystal electromagnetic calorimeter, and a brass and scintillator hadron calorimeter. Muons are measured in gas-ionization detectors embedded in the steel flux-return yoke outside the solenoid, with detection planes are made using three technologies: drift tubes, cathode strip chambers, and resistive-plate chambers. Muons are measured in the pseudorapidity range $|\eta| < 2.4$.

The silicon tracker measures charged particles within the pseudorapidity range $|\eta| < 2.5$. It consists of 1440 silicon pixel and 15 148 silicon strip detector modules and provides a typical transverse impact parameter resolution of 25–90 μm. Matching muons to tracks measured in the silicon tracker results in a transverse momentum resolution between 1% and 2.8%, for p_T

values up to 100 GeV [17].

The first level of the CMS trigger system, composed of custom hardware processors, uses information from the calorimeters and muon detectors to select the most interesting events in a fixed time interval of less than $4\,\mu$s. The high-level trigger processor farm further decreases the event rate from around 100 kHz to around 400 Hz, before data storage. A more detailed description of the CMS detector, together with a definition of the coordinate system used and the relevant kinematic variables, can be found in Ref. [18].

3 Differential cross section measurement methodology

Event selection starts with a dimuon trigger involving the silicon tracker and muon systems. The trigger, which is exposed to the full integrated luminosity, requires at least two muons with dimuon rapidity $|y| < 1.25$, dimuon invariant mass $8.5 < M_{\mu\mu} < 11.5$ GeV, and a dimuon vertex fit with a χ^2 probability $>0.5\%$. The trigger selects only pairs of muons that bend away from each other in the magnetic field ("seagull selection"), i.e., events for which the difference in azimuthal angle between the positively charged and negatively charged muons is less than zero. Requiring that muon trajectories do not cross in the transverse plane improves the muon efficiency. Trigger p_{T} thresholds varied from 5–9 GeV as the beam conditions changed. Offline selection criteria required $p_{\mathrm{T}} > 10$ GeV, $|y| < 1.2$, and a dimuon vertex fit χ^2 probability $>1\%$. Standard CMS quality requirements are used to identify muons and muons are restricted to $|\eta(\mu)| < 1.6$. The muon tracks are required to have at least ten hits in the silicon tracker, at least one hit in the silicon pixel detector, and be matched with at least one segment of the muon system. The muon track fit quality must have a χ^2 per degree of freedom of less than 1.8. The distance of the track from the closest primary vertex must be less than 15 cm in the longitudinal direction and 3 cm in the transverse direction. The following kinematic requirements are also imposed to ensure accurate muon detection efficiency evaluation:

$$
\begin{aligned}
p_{\mathrm{T}}(\mu) &> 3\,\text{GeV} &&\text{for } 1.4 < |\eta(\mu)| < 1.6, \\
p_{\mathrm{T}}(\mu) &> 3.5\,\text{GeV} &&\text{for } 1.2 < |\eta(\mu)| < 1.4, \\
p_{\mathrm{T}}(\mu) &> 4.5\,\text{GeV} &&\text{for } |\eta(\mu)| < 1.2.
\end{aligned}
\tag{1}
$$

The differential cross sections are measured for two rapidity ranges: $|y| \leq 0.6$ and $0.6 < |y| < 1.2$, as well as for the entire range $|y| < 1.2$. In each rapidity range the data are binned in p_{T}, with bin edges at 2 GeV intervals between 10 and 40 GeV, then wider bins with edges at 43, 46, 50, 55, 60, 70, and 100 GeV.

The Y(nS) differential cross section times dimuon branching fraction, integrated over either of the two $|y|$ ranges and in a given p_{T} bin of width Δp_{T}, is

$$
\frac{\mathrm{d}\sigma\big(\mathrm{pp} \to \mathrm{Y}(n\mathrm{S})\big)}{\mathrm{d}p_{\mathrm{T}}}\bigg|_{|y|\text{ range}} \mathcal{B}\big(\mathrm{Y}(n\mathrm{S}) \to \mu^+\mu^-\big) = \frac{N^{\mathrm{fit}}_{\mathrm{Y}(n\mathrm{S})}(p_{\mathrm{T}})}{L\Delta p_{\mathrm{T}}\epsilon_{\mu\mu}(p_{\mathrm{T}})\mathcal{A}(p_{\mathrm{T}})\epsilon_{\mathrm{sg}}\epsilon_{\mathrm{vp}}},
\tag{2}
$$

where $N^{\mathrm{fit}}_{\mathrm{Y}(n\mathrm{S})}$ is the fitted number of Y(nS) events from the dimuon invariant mass distribution in a p_{T} bin for the selected $|y|$ range, $\epsilon_{\mu\mu}$ is the dimuon efficiency, L is the integrated luminosity, $\mathcal{A}$ is the polarization-corrected acceptance, ϵ_{sg} is the efficiency of the seagull selection, and ϵ_{vp} is the efficiency of the dimuon vertex χ^2 probability requirement. The efficiency and acceptance determinations are described below.

The total yield $N^{\text{fit}}_{\text{Y}(n\text{S})}$ for the three Y(nS) states in the rapidity range $|y| < 1.2$ are $412\,900 \pm 600$ Y(1S) events, $151\,700 \pm 400$ Y(2S) events, and $111\,100 \pm 300$ Y(3S) events, where the uncertainties are statistical only. The fine granularity of the CMS tracker kept the efficiency independent of changes in the LHC instantaneous luminosity throughout the $\sqrt{s} = 7\,\text{TeV}$ operations.

3.1   Efficiency factors

The dimuon efficiency for a given event is parameterized as:

$$\epsilon_{\mu\mu} \equiv \epsilon_1[p_{\text{T}}(\mu_1), \eta(\mu_1)]\, \epsilon_2[p_{\text{T}}(\mu_2), \eta(\mu_2)]\, \rho, \tag{3}$$

where $\epsilon_i[p_{\text{T}}(\mu_i), \eta(\mu_i)]$ is the overall single-muon quality and trigger efficiency. The kinematic dependence of the ρ factor was determined in a study based on Monte Carlo (MC) simulation using EVTGEN [19] with a detector simulation performed with GEANT4 [20]. The parameter ρ accounts for the possibility that two genuine muons can be merged during the reconstruction or trigger selection, causing an inefficiency. It was found to depend on the quadrature sum of the differences $\Delta p_{\text{T}}/(637\,\text{GeV})$, $\Delta\eta$, and $1.2\Delta\phi$ between the two muons. The MC simulation result was validated by measuring the ρ factor with Y(nS) events reconstructed using a data set that required only a single-muon trigger. In events such as those with $p_{\text{T}} < 50\,\text{GeV}$, where the muons are well separated, $\rho = 1$. For high-p_{T} events of $p_{\text{T}} > 80\,\text{GeV}$, where the muons are closer together, ρ drops to approximately 0.7.

The single-muon efficiencies are measured using the tag-and-probe approach based on control samples in data, as described in Ref. [21], times the tracking efficiency (0.99 ± 0.01), determined from MC simulation. We assume that the dimuon efficiency within each Y(nS) mass region is the same for signal and background. The dimuon efficiency $\epsilon_{\mu\mu}$ for a given $(p_{\text{T}}, |y|)$ is obtained by averaging the calculated event dimuon efficiency $\epsilon_{\mu\mu}$ for each data event in the bin. This is done separately for the three Y states, using a mass range of $\pm 200\,\text{MeV}$ for the Y(1S) and $\pm 100\,\text{MeV}$ for the higher-mass states. The narrower range for the Y(2S) and Y(3S) states is chosen because of the closeness in mass of these two states. The average efficiency, $\epsilon_{\mu\mu}$, is typically 0.75–0.80. For all (p_{T}, y) bins the systematic difference between averaging in $\epsilon_{\mu\mu}$ or $1/\epsilon_{\mu\mu}$ can be neglected in comparison to the quoted systematic uncertainty due to the single muon efficiencies. To determine ϵ_{sg}, we note that there is a 50% probability that a Y(nS) state will decay in the seagull configuration. It was verified in MC simulation that $\epsilon_{\text{sg}} = 0.5$. The efficiency ϵ_{vp} for the dimuon vertex fit χ^2 probability requirement is determined to be 0.99 ± 0.01 from MC simulation, where the uncertainty is statistical. This efficiency was validated in data using events from a trigger that did not require vertex selection. We also computed the total acceptance and efficiency product in the MC simulation and compared it with the result based on the factorized approach. The results agreed over the entire p_{T} range of the measurement.

3.2   Acceptance

For each Y(nS) state the acceptance $\mathcal{A}$ is computed in each $(p_{\text{T}}, |y|)$ bin and defined as the fraction of its dimuon decays that satisfy the single-muon kinematic selections given by Eq. (1). The acceptances are computed using generator-level muons, then repeated using reconstructed muons in the full simulation study. The results agree to better than 2% at all p_{T} values. Differences are contained within the systematic uncertainty band (Section 4.3) assigned for the muon reconstruction. To account for the effect of the Y(nS) polarization on the muon angular

distribution, each MC simulation event is weighted by an angular factor w:

$$w = \frac{3}{4\pi} \left(\frac{1}{3+\lambda_\theta} \right) \left(1 + \lambda_\theta \cos^2\theta + \lambda_\phi \sin^2\theta \cos 2\phi + \lambda_{\theta\phi} \sin 2\theta \cos\phi \right),$$ (4)

where $\lambda_\theta, \lambda_\phi, \lambda_{\theta\phi}$ are the measured polarization parameters [5], θ is the polar angle, and ϕ the azimuthal angle of the positively charged muon in the $\Upsilon(nS)$ helicity frame (HX). The polarization was measured in the range $10 < p_T < 50\,\text{GeV}$ in the same two rapidity bins as this analysis. The measured polarization parameters do not show a statistically significant dependence on p_T. We linearly interpolate each of the measured polarization parameters in p_T. Linear interpolation is also used for the 68.3% confidence level (CL) uncertainties in the polarization measurements to determine the uncertainty in the three parameters from the analysis. The polarization parameters for $p_T > 50\,\text{GeV}$ are taken to be the average of the measured values for $10 < p_T < 50\,\text{GeV}$. The largest measured absolute uncertainty for each parameter is used for the extrapolated uncertainties because the spread in nominal values is small. The acceptance is computed initially using a flat p_T distribution within a bin, then reweighted after fitting the measured p_T distribution to a functional form (see Section 5). The acceptances in each p_T bin for the three rapidity intervals are given in Appendix A (Tables A.7–A.15) for the measured polarization central value and the 68.3% CL uncertainties on the parameters [5]. In addition, we report the acceptance computed for the hypotheses of zero, 100% transverse, and 100% longitudinal polarization that correspond to the parameter values $\lambda_\phi = \lambda_{\theta\phi} = 0$ and $\lambda_\theta = 0, +1$, and -1 respectively. Because of the agreement in the acceptance when computed with generator-level and reconstructed muons, the cross section results reported here can be scaled to accommodate any other polarization by using a generator-level MC simulation with a given polarization.

4   Yield determination procedure

4.1   Lineshape determination

The $\Upsilon(nS)$ lineshape is determined using the measured muon momenta and their uncertainties, along with a generator-level simulated invariant mass (SIM) distribution including final-state radiation (FSR) effects. For events in a given $(p_T, |y|)$ bin, the distribution of the dimuon invariant mass uncertainty ζ is computed from the muon track error matrices.

In order to describe the $\Upsilon(nS)$ SIM distribution without detector resolution effects, we simulate dimuon events for a given $\Upsilon(nS)$ state using EVTGEN and compute the FSR using PHOTOS [22, 23]. The standard PHOTOS minimum photon energy for the $\Upsilon(nS)$ states is ≈ 50 MeV, which is of the same order as our dimuon invariant mass uncertainty. To improve the description, we extend the photon energy spectrum down to 2 MeV using a fit of the SIM distribution to the QED inner-bremsstrahlung formula [23]. The systematic uncertainties of the soft photon approximation in PHOTOS compared to exact QED calculations are discussed in Ref. [23]. For the range of photon energies expected in $\Upsilon(nS)$ decays the systematic uncertainty is negligible.

In each rapidity range, the $\Upsilon(nS)$ lineshape for a given p_T bin is expressed by a probability density function (PDF) for the signal dimuon mass $M_{\mu\mu}$. This function $\mathcal{F}(M_{\mu\mu}; c_w, \delta m)$ is the average of N values of the dimuon mass m_i smeared with a resolution ζ_i:

$$\mathcal{F}(M_{\mu\mu}; c_w, \delta m) = \frac{1}{N} \sum_{i=1}^{N} \frac{1}{\sqrt{2\pi}c_w\zeta_i} e^{-(M_{\mu\mu}-m_i-\delta m)^2/2c_w^2\zeta_i^2}.$$ (5)

Each $\Upsilon(nS)$ state is handled in the same fashion. Values of m_i and ζ_i are selected by randomly sampling the radiative mass function and the ζ distribution for that $(p_T, |y|)$ bin. Two correction

factors are common to all three $\Upsilon(nS)$ peaks in a given $(p_\mathrm{T}, |y|)$ bin: a width scale factor c_w, to correct for any ζ scale difference between data and the MC simulation, and a mass-shift δm, to correct for any difference in p_T scale between data and the MC simulation. We sample $N = 25\,000$ (m_i, ζ_i) points per p_T bin, stored in a histogram with $0.25\,\mathrm{MeV}$ bins to smooth the fluctuations and retain shape features. This histogram gives the normalized, resolution-smeared mass PDF for a given $\Upsilon(nS)$ state in a particular $(p_\mathrm{T}, |y|)$ bin. The procedure was validated in MC simulation by generating the lineshape using a subset of generated $\Upsilon(1S)$ events, then fitting the rest of the events with that lineshape. The fitted number of events was consistent with the generated number.

4.2 Fitting for yields

To determine the yields of the three states in each p_T and $|y|$ range requires a fit to the dimuon mass distribution in every $(p_\mathrm{T}, |y|)$ bin. The total PDF for $M_{\mu\mu}$ describes the signal and background contributions to the dimuon invariant mass distribution using a signal PDF as defined in Eq. (5) for each of the $\Upsilon(nS)$ states, plus a background function. Four background functions are studied: an exponential and a Chebyshev series with maximum order of 0, 1, or 2.

We measure the yield by performing an extended maximum-likelihood fit using ROOFIT [24] to determine the number of signal events associated with each normalized signal PDF. To allow cancellation of some common uncertainties in the muon acceptance and efficiency calculation in the measurement of the ratios of $\Upsilon(2S)$ and $\Upsilon(3S)$ differential cross sections to that of the $\Upsilon(1S)$, we perform an additional fit normalized to the $\Upsilon(1S)$ yield. For each p_T bin the optimal background function is determined using the Akaike Information Criterion (AIC) [25], taking the function with the largest relative probability, as discussed in Ref. [26]. This method is similar to a maximum-likelihood evaluation, but it adds a term equal to twice the number of free parameters in the fit, thus penalizing addition of free parameters. The parameters c_w and δm are determined from the fit for each p_T bin. Typical values and corresponding uncertainties for c_w and δm are 1.04 ± 0.01 and $3 \pm 1\,\mathrm{MeV}$, respectively. The fit correlation matrix shows that their influence on the yields is a small fraction of the statistical uncertainty in each yield.

The plots in Fig. 1 show two examples of fitting the dimuon invariant mass distribution using the lineshape method. The lower plots show the pull, $(N_\mathrm{data} - N_\mathrm{fit})/\sigma_\mathrm{data}$, in each dimuon mass bin, where N_data is the observed number of events in the bin, N_fit is the integral of the fitted signal and background function in that bin, and the uncertainty σ_data is the Poisson statistical uncertainty. As can be seen in Fig. 1, the lineshape description represents the data well, even at high p_T and large rapidity.

4.3 Systematic uncertainties

The overall systematic uncertainty in the cross section for a given $(p_\mathrm{T}, |y|)$ bin includes uncertainties from the background fit method, the lineshape determination, the dimuon efficiency, the acceptance variations due to varying the polarization parameters within their 68.3% CL ranges, and the integrated luminosity. The systematic uncertainty from the background function is estimated using the maximum difference in yields among background functions with an AIC probability above 5% [25, 26] relative to the best background choice. An upper limit of 1% on the systematic uncertainty from the lineshape function determination for all three $\Upsilon(nS)$ states and all $(p_\mathrm{T}, |y|)$ bins is estimated by varying the width of the mass region in which the mass resolution parameter ζ is determined. The efficiency systematic is evaluated by modifying $\epsilon_{\mu\mu}$ event by event, using the ± 1 standard deviation values from the tag-and-probe measurements [5]. There is a 1% systematic uncertainty to account for small variations in $\epsilon_{\mu\mu}$ as a function of $M_{\mu\mu}$ observed in the data. The measured ρ factor values from the experimental
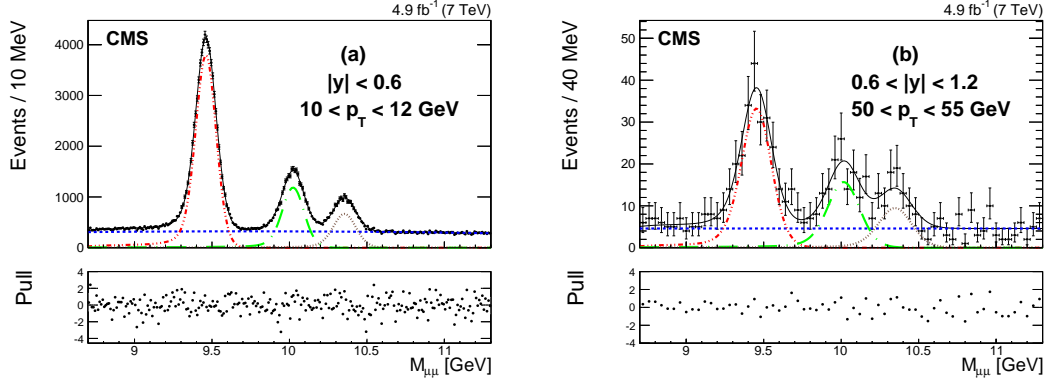
Figure 1: Results of the fits to the dimuon invariant mass distribution for events in two bins: (a): $|y| < 0.6$, $10 < p_T < 12\,\text{GeV}$ and (b): $0.6 < |y| < 1.2$, $50 < p_T < 55\,\text{GeV}$. The solid line is the result of the full fit. The dash-dotted line is the Y(1S) signal fit, the long-dashed line is the Y(2S) signal fit, and the dotted line is the Y(3S) signal fit. The short-dashed line is the background contribution. The lower plots show the pull for each mass bin.

determination and from MC simulation agree over the full p_T range. We assign a systematic uncertainty for ρ of 0.5–5%, which equals the full difference between the MC simulation and the experimental measurement. We compute the acceptance systematic uncertainty by raising and lowering all three polarization parameters by their interpolated 68.3% CL values from Ref. [5]. The resulting 5–8% change in the acceptance is used as the systematic uncertainty in the acceptance as tabulated in Appendix A (Tables A.7–A.15). The total systematic uncertainty is found from the quadrature sum of the individual systematic uncertainties. It is comparable to or smaller than the statistical uncertainty for $p_T > 40\,\text{GeV}$. There is a 2.2% uncertainty [27] from the integrated luminosity determination that applies to all p_T bins. This uncertainty is not included in the uncertainties displayed in the figures or given in the tables.

5   Results

The measured Y(nS) differential cross sections versus p_T are shown in Fig. 2 over the full rapidity range $|y| < 1.2$. The vertical bars on the points in Fig. 2 show the statistical and systematic uncertainties added in quadrature. Earlier CMS measurements [2] are shown for comparison, scaled by 0.5 to account for the smaller $|y|$ range in the latest measurement, where the scaling assumes that the rapidity distribution is flat. The Y(nS) differential cross sections peak near $p_T = 4\,\text{GeV}$, as seen in Fig. 2. Their shape can be described by an exponential function for $10 \lesssim p_T \lesssim 20\,\text{GeV}$, while for $p_T \gtrsim 20\,\text{GeV}$ the data lie above the exponential and the slope changes. Therefore, we fit the high-p_T measurements for each Y(nS) state using a power-law parametrization:

$$\frac{d\sigma\left(pp \to Y(nS)\right)}{dp_T}\Bigg|_{|y|\text{ range}} \mathcal{B}\left(Y(nS) \to \mu^+\mu^-\right) = \frac{A}{C + \left(\frac{p_T}{p_0}\right)^\alpha}, \tag{6}$$

where A is a normalization with units of pb/GeV. The value of p_0 is fixed to 20 GeV and has no influence on the exponent α, which describes the curvature of the function. The differential cross section fits are evaluated using the integral value of the function over the p_T range of each bin, and the results are given in Table 1. The bin centers are determined by the functional-weight method described in [28], using the exponential fit for $p_T < 20\,\text{GeV}$ and the power-law

form in Eq. 6 for $p_T > 20$ GeV. Shifts from the p_T-weighted mean values are negligible in all except the highest-p_T bin, where using the functional weight moves the bin center from 79 to 82 GeV. Tables A.1–A.3 in Appendix A give the measured values shown in Fig. 2 as well as for the two rapidity ranges $|y| < 0.6$ and $0.6 < |y| < 1.2$.

To illustrate the quality of this functional description, Fig. 2 (b) shows the fit results for the $\Upsilon(1S)$ state with $|y| < 1.2$. The solid line is the power-law fit for $p_T > 20$ GeV. The dashed line is the exponential fit for $10 < p_T < 20$ GeV. The lower plot shows, for each p_T bin, the pull determined from the differential cross section value in a (p_T, $|y|$) bin and its total uncertainty.

Table 1: The values of the parameters in Eq. (6) from the power-law fit to $\Upsilon(1S)$ events with $p_T > 20$ GeV and $|y| < 1.2$, along with the χ^2 value and the number of degrees of freedom n_d.

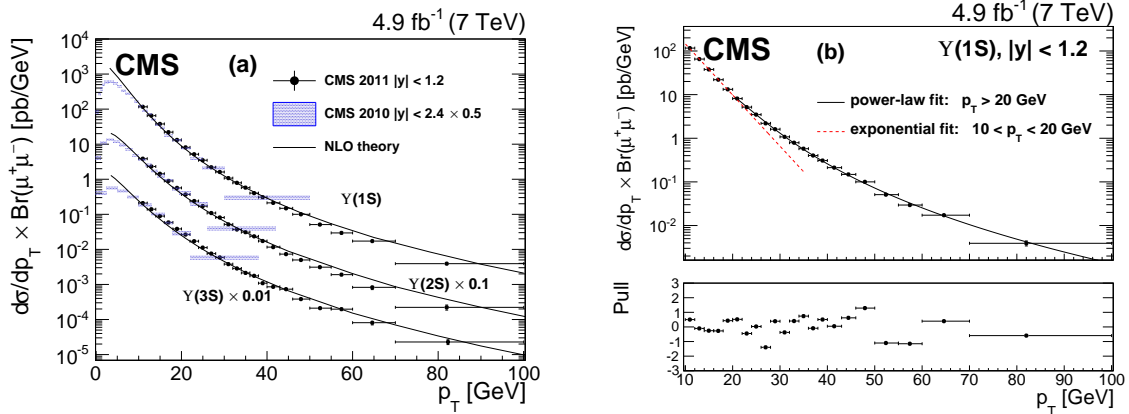|	$\Upsilon(1S)$	$\Upsilon(2S)$	$\Upsilon(3S)$
A	14.00 ± 0.75	6.88 ± 0.48	4.01 ± 0.30
α	5.75 ± 0.07	5.62 ± 0.10	5.26 ± 0.10
C	0.45 ± 0.13	0.62 ± 0.18	0.26 ± 0.15
χ^2	8.7	11	15
n_d	14	14	14

Figure 2: (a) The $\Upsilon(nS)$ differential p_T cross sections times dimuon branching fractions for $|y| < 1.2$. The $\Upsilon(2S)$ and $\Upsilon(3S)$ measurements are scaled by 0.1 and 0.01, respectively, for display purposes. The vertical bars show the total uncertainty, excluding the systematic uncertainty in the integrated luminosity. The horizontal bars show the bin widths. Previous CMS measurements for $|y| < 2.4$ are shown as cross-hatched areas [2]. These results have been scaled by 0.5 to account for the smaller $|y|$ range in the latest measurement, where the scaling assumes that the rapidity distribution is flat. The solid lines are the NLO calculations from Ref. [13] extended by the authors to cover the range $p_T < 100$ GeV. (b) Details of the parametrized cross section fit described in the text for $\Upsilon(1S)$ with $|y| < 1.2$. In this plot the solid line is the result of the power-law fit (see Eq. 6) for $p_T > 20$ GeV. The dashed line shows an exponential fit to the data for $10 < p_T < 20$ GeV. The lower plot shows the pulls of the fit as defined in the text.

Next, we consider the p_T dependence of the ratios of the $\Upsilon(nS)$ production cross sections times their dimuon branching fractions. The yield fits are redone to compute explicitly the yield ratio r_{21} for $\Upsilon(2S)$ to $\Upsilon(1S)$ and r_{31} for $\Upsilon(3S)$ to $\Upsilon(1S)$. The efficiency ratio is computed for each (p_T, $|y|$) bin. The polarization-weighted acceptance and its uncertainty is computed for each state separately, and the uncertainties are added in quadrature to determine the uncertainty in the ratio. The corrected yield ratios are $R_{n1}(p_T, |y|) = r_{n1}(p_T, |y|) \, (\mathcal{A}_1 \epsilon_1)/(\mathcal{A}_n \epsilon_n)$, where $n = 2, 3$.

The measured corrected ratios are shown in Fig. 3 and given in Appendix A (Tables A.4–A.6). The rapid rise of both ratios for $p_T < 20\,\text{GeV}$ slows significantly for $p_T \gtrsim 20\,\text{GeV}$. The curves on the ratio plots are the ratios of the corresponding fitted functions from the individual $\Upsilon(n\text{S})$ differential cross section fits (exponential for $p_T < 20\,\text{GeV}$, power-law for $p_T > 20\,\text{GeV}$). The curves confirm that the change in ratios occurs in the same p_T range in which $d\sigma/dp_T$ also changes behavior.

The measurements for the ratio R_{31} in Fig. 3(b), found in the supplementary material, can be fit to a linear function and to a constant in order to quantify the visual evidence that the $\Upsilon(3\text{S})$ production is harder than that of the $\Upsilon(1\text{S})$. The linear fit to measurements with $p_T > 20\,\text{GeV}$ has χ^2 probability 0.22, while the fit to a constant has χ^2 probability 2.6×10^{-5}. Thus, with relative probability 85000:1, we can say that $\Upsilon(3\text{S})$ production is harder than that of the $\Upsilon(1\text{S})$. The $\Upsilon(2\text{S})/\Upsilon(1\text{S})$ production ratio versus p_T has a similar trend, but the statistical uncertainties are too large to make a definite statement.
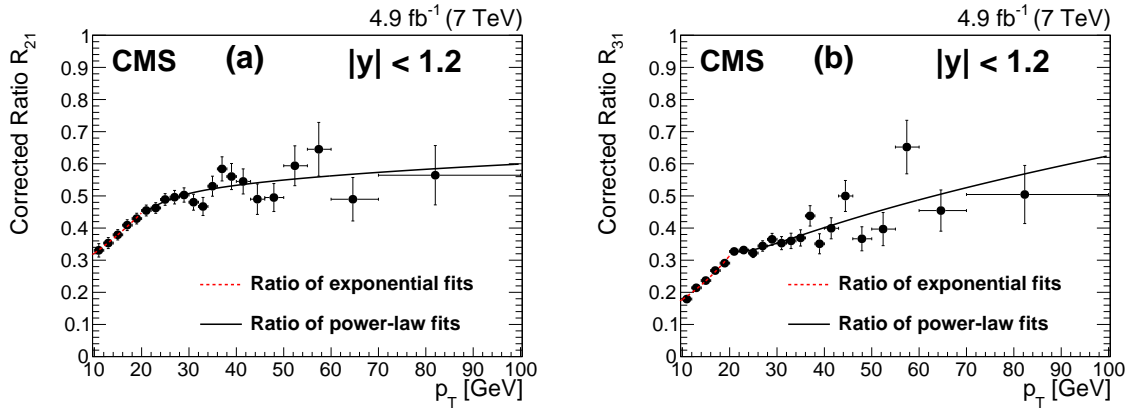

Figure 3: Measured differential cross section ratios as a function of p_T. Corrected yield ratios: (a) R_{21}; (b) R_{31}. The dashed line is the ratio of the exponential fits to the individual differential cross sections for $10 < p_T < 20\,\text{GeV}$. The solid line is the ratio of the corresponding power-law fits for $p_T > 20\,\text{GeV}$.

6   Discussion

Theoretical predictions for the $\Upsilon(n\text{S})$ differential cross sections have been previously compared to the first LHC cross section measurements [10, 14, 15]. A more recent CMS measurement [2] included the currently available predictions from the CSM [14], valid for $p_T < 35\,\text{GeV}$, and an unpublished NRQCD prediction that covers the range $p_T < 30\,\text{GeV}$. The NRQCD + NLO analysis from Ref. [13] describes $\Upsilon(n\text{S})$ production at Tevatron and LHC energies for $p_T < 50\,\text{GeV}$. An extension of these predictions to $p_T = 100\,\text{GeV}$ is compared to the CMS measurements in Fig. 2 (a). The calculations describe the trends of the data for all three $\Upsilon(n\text{S})$ states.

The color evaporation model (CEM), a variant of the CSM, predicts that above a minimum $p_T \approx M_{\Upsilon(1\text{S})}$, all bottomonium states should have the same p_T dependence [29]. The measured ratios of the differential cross sections as a function of p_T in Fig. 3 show that this is not the case for p_T less than about $40\,\text{GeV}$.

Changing the $\Upsilon(n\text{S})$ p_T threshold for the data used in calculating the NRQCD predictions results in different LDMEs [10, 30, 31]. Recent theoretical work [12, 16] has demonstrated the impact of varying the p_T thresholds in NRQCD analyses to study different production amplitude behavior. These new CMS data provide a significant extension of the p_T range that can

be used in evaluating matrix elements and studying p_T-dependent corrections in NRQCD and other models. The new results on Y(3S) production are sufficiently accurate to allow one to focus model building of the p_T behavior on that state, for which feeddown contributions come only from the χ_b(3P).

7 Summary

Measurements of the differential production cross sections as a function of p_T for the Y(1S), Y(2S), and Y(3S) states in pp collisions at $\sqrt{s} = 7\,\text{TeV}$ have been presented, based on a data sample corresponding to an integrated luminosity of $4.9\,\text{fb}^{-1}$ collected by the CMS experiment at the LHC. Not only do these measurements significantly improve the precision of the results in previously analyzed p_T ranges [1–3], they also extend the maximum p_T range from 70 to 100 GeV. Evidence has been presented for the first time of the power-law nature of the p_T distributions for all three Y(nS) states at high p_T. Combined with the CMS Y(nS) polarization results [5], the new bottomonium measurements are a formidable challenge to our theoretical understanding of the production of heavy-quark bound states.

Acknowledgments

References

[1] CMS Collaboration, "Measurement of the inclusive Υ production cross section in pp collisions at $\sqrt{s} = 7$ TeV", *Phys. Rev. D* **83** (2011) 112004, `doi:10.1103/PhysRevD.83.112004`, `arXiv:1012.5545`.

[2] CMS Collaboration, "Measurement of the $\Upsilon(1S)$, $\Upsilon(2S)$, and $\Upsilon(3S)$ cross sections in pp collisions at $\sqrt{s} = 7$ TeV", *Phys. Lett. B* **727** (2013) 101, `doi:10.1016/j.physletb.2013.10.033`, `arXiv:1303.5900`.

[3] ATLAS Collaboration, "Measurement of upsilon production in 7 TeV pp collisions at ATLAS", *Phys. Rev. D* **87** (2013) 052004, `doi:10.1103/PhysRevD.87.052004`, `arXiv:1211.7255`.

[4] LHCb Collaboration, "Measurement of Υ production in pp collisions at $\sqrt{s} = 7$ TeV", *Eur. Phys. J. C* **72** (2012) 2025, `doi:10.1140/epjc/s10052-012-2025-y`, `arXiv:1202.6579`.

[5] CMS Collaboration, "Measurement of the $\Upsilon(1S)$, $\Upsilon(2S)$ and $\Upsilon(3S)$ Polarizations in pp Collisions at $\sqrt{s} = 7$ TeV", *Phys. Rev. Lett.* **110** (2013) 081802, `doi:10.1103/PhysRevLett.110.081802`, `arXiv:1209.2922`.

[6] D0 Collaboration, "Measurement of Inclusive Differential Cross Sections for $\Upsilon(1S)$ Production in $p\bar{p}$ Collisions at $\sqrt{s} = 1.96$ TeV", *Phys. Rev. Lett.* **94** (2005) 232001, `doi:10.1103/PhysRevLett.94.232001`, `arXiv:hep-ex/0502030`. [Erratum: `doi:10.1103/PhysRevLett.100.049902`].

[7] CDF Collaboration, "Υ Production and Polarization in $p\bar{p}$ Collisions at $\sqrt{s} = 1.8$ TeV", *Phys. Rev. Lett.* **88** (2002) 161802, `doi:10.1103/PhysRevLett.88.161802`.

[8] P. L. Cho and A. K. Leibovich, "Color octet quarkonia production", *Phys. Rev. D* **53** (1996) 150, `doi:10.1103/PhysRevD.53.150`, `arXiv:hep-ph/9505329`.

[9] P. L. Cho and A. K. Leibovich, "Color octet quarkonia production. II", *Phys. Rev. D* **53** (1996) 6203, `doi:10.1103/PhysRevD.53.6203`, `arXiv:hep-ph/9511315`.

[10] K. Wang, Y.-Q. Ma, and K.-T. Chao, "$\Upsilon(1S)$ prompt production at the Tevatron and LHC in nonrelativistic QCD", *Phys. Rev. D* **85** (2012) 114003, `doi:10.1103/PhysRevD.85.114003`, `arXiv:1202.6012`.

[11] G. T. Bodwin et al., "Quarkonium at the Frontiers of High Energy Physics: A Snowmass White Paper", (2013). `arXiv:1307.7425`.

[12] G. T. Bodwin, H. S. Chung, U.-R. Kim, and J. Lee, "Fragmentation Contributions to J/ψ Production at the Tevatron and the LHC", *Phys. Rev. Lett.* **113** (2014) 022001, `doi:10.1103/PhysRevLett.113.022001`, `arXiv:1403.3612`.

[13] B. Gong, L.-P. Wan, J.-X. Wang, and H.-F. Zhang, "Complete Next-to-Leading-Order Study on the Yield and Polarization of Υ(1S, 2S, 3S) at the Tevatron and LHC", *Phys. Rev. Lett.* **112** (2014) 032001, `doi:10.1103/PhysRevLett.112.032001`, `arXiv:1305.0748`.

[14] P. Artoisenet et al., "Υ Production at Fermilab Tevatron and LHC Energies", *Phys. Rev. Lett.* **101** (2008) 152001, `doi:10.1103/PhysRevLett.101.152001`, `arXiv:0806.3282`.

[15] S. P. Baranov, "Prompt $\Upsilon(nS)$ production at the LHC in view of the k_t-factorization approach", *Phys. Rev. D* **86** (2012) 054015, `doi:10.1103/PhysRevD.86.054015`.

[16] P. Faccioli et al., "Quarkonium production in the LHC era: a polarized perspective", *Phys. Lett. B* **736** (2014) 98, `doi:10.1016/j.physletb.2014.07.006`, `arXiv:1403.3970`.

[17] CMS Collaboration, "Performance of CMS muon reconstruction in pp collision events at $\sqrt{s} = 7$ TeV", *JINST* **7** (2012) P10002, `doi:10.1088/1748-0221/7/10/P10002`, `arXiv:1206.4071`.

[18] CMS Collaboration, "The CMS experiment at the CERN LHC", *JINST* **3** (2008) S08004, `doi:10.1088/1748-0221/3/08/S08004`.

[19] D. J. Lange, "The EvtGen particle decay simulation package", *Nucl. Instrum. Meth. A* **462** (2001) 152, `doi:10.1016/S0168-9002(01)00089-4`.

[20] GEANT4 Collaboration, "GEANT4—a simulation toolkit", *Nucl. Instrum. Meth. A* **506** (2003) 250, `doi:10.1016/S0168-9002(03)01368-8`.

[21] CMS Collaboration, "Measurements of inclusive W and Z cross sections in pp collisions at $\sqrt{s} = 7$ TeV", *JHEP* **01** (2011) 080, `doi:10.1007/JHEP01(2011)080`, `arXiv:1012.2466`.

[22] E. Barberio, B. van Eijk, and Z. Wąs, "PHOTOS: A universal Monte Carlo for QED radiative corrections in decays", *Comput. Phys. Commun.* **66** (1991) 115, `doi:10.1016/0010-4655(91)90012-A`.

[23] E. Barberio and Z. Wąs, "PHOTOS: A universal Monte Carlo for QED radiative corrections: Version 2.0", *Comput. Phys. Commun.* **79** (1994) 291, `doi:10.1016/0010-4655(94)90074-4`.

[24] W. Verkerke and D. P. Kirkby, "The RooFit toolkit for data modeling", in *2003 Computing in High Energy and Nuclear Physics (CHEP03)*, p. 186. 2003. `arXiv:physics/0306116`. eConf C0303241 (2003) MOLT007.

[25] H. Akaike, "A new look at the statistical model identification", *IEEE Transactions on Automatic Control* **19** (1974) 716, `doi:10.1109/TAC.1974.1100705`.

[26] K. Burnham and D. Anderson, "Multimodel Inference: Understanding AIC and BIC in Model Selection", *Sociological Methods Research* **33** (2004) 261, `doi:10.1177/0049124104268644`.

[27] CMS Collaboration, "Absolute Calibration of the Luminosity Measurement at CMS: Winter 2012 Update", CMS Physics Analysis Summary CMS-PAS-SMP-12-008, 2012.

[28] G. D. Lafferty and T. R. Wyatt, "Where to stick your data points: The treatment of measurements within wide bins", *Nucl. Instrum. Meth. A* **355** (1995) 541, `doi:10.1016/0168-9002(94)01112-5`.

[29] J. F. Amundson, O. J. P. Eboli, E. M. Gregores, and F. Halzen, "Colorless states in perturbative QCD: Charmonium and rapidity gaps", *Phys. Lett. B* **372** (1996) 127, `doi:10.1016/0370-2693(96)00035-4`, `arXiv:hep-ph/9512248`.

[30] M. Butenschoen and B. A. Kniehl, "World data of J/ψ production consolidate NRQCD factorization at NLO", *Phys. Rev. D* **84** (2011) 051501, `doi:10.1103/PhysRevD.84.051501,arXiv:1105.0820`.

[31] M. Butenschoen and B. A. Kniehl, "Reconciling J/ψ production at HERA, RHIC, Tevatron, and LHC with NRQCD factorization at next-to-leading order", *Phys. Rev. Lett.* **106** (2011) 022003, `doi:10.1103/PhysRevLett.106.022003,arXiv:1009.5662`.

A Supplementary material

Table A.1: The p_T bin width, the weighted mean p_T within a bin, and the differential cross section times the dimuon branching fraction: $(d\sigma/dp_T)\mathcal{B}(Y(nS) \rightarrow \mu^+\mu^-)$ for the Y(1S), Y(2S), and Y(3S) with $0 < |y| < 0.6$. The statistical uncertainty in the differential cross section is given as the percentage of the cross section in the format: $\sigma_{stat}/(d\sigma/dp_T)$ (%) and similarly for the systematic uncertainty. The percentage systematic uncertainty for a negative systematic shift is given in parentheses. The statistical uncertainties are derived from the fit to the dimuon mass spectrum. The systematic uncertainties are discussed in the text. The 2.2% systematic uncertainty in the integrated luminosity is not included.

p_T	$\langle p_T \rangle$	$\frac{d\sigma}{dp_T}\mathcal{B}$	$\frac{\sigma_{stat}}{d\sigma/dp_T}$	$\frac{\sigma_{syst}}{d\sigma/dp_T}$	$\frac{d\sigma}{dp_T}\mathcal{B}$	$\frac{\sigma_{stat}}{d\sigma/dp_T}$	$\frac{\sigma_{syst}}{d\sigma/dp_T}$	$\frac{d\sigma}{dp_T}\mathcal{B}$	$\frac{\sigma_{stat}}{d\sigma/dp_T}$	$\frac{\sigma_{syst}}{d\sigma/dp_T}$
		Y(1S)			**Y(2S)**			**Y(3S)**		
GeV	GeV	(fb/GeV)	(%)	(%)	(fb/GeV)	(%)	(%)	(fb/GeV)	(%)	(%)
10–12	11.0	60936	0.5	6.8 (7.2)	20036	1.0	8.6 (9.4)	10951	1.4	10.0 (11.3)
12–14	13.0	33828	0.5	5.1 (5.6)	12072	1.1	6.0 (6.7)	7181	1.4	7.1 (8.0)
14–16	15.0	19670	0.6	4.8 (5.2)	7621	1.2	5.2 (5.7)	4596	1.6	5.7 (6.3)
16–18	17.0	11504	0.8	4.6 (4.9)	4858	1.3	5.1 (5.5)	3097	1.7	5.6 (6.1)
18–20	19.0	6914	0.9	4.5 (4.7)	3034	1.5	4.9 (5.2)	1966	2.0	5.2 (5.6)
20–22	21.0	4235	1.1	4.2 (4.4)	1932	1.8	4.6 (4.9)	1423	2.2	5.0 (5.2)
22–24	23.0	2721	1.4	4.1 (4.3)	1203	2.3	4.5 (4.6)	893	2.7	4.7 (4.9)
24–26	25.0	1848	1.7	4.1 (4.2)	849	2.6	4.6 (4.7)	594	3.3	4.9 (5.1)
26–28	27.0	1117	2.2	4.3 (4.4)	537	3.6	5.7 (5.8)	381	4.4	6.1 (6.2)
28–30	29.0	845	2.5	4.4 (4.5)	413	4.0	5.8 (5.8)	314	4.7	6.0 (6.1)
30–32	31.0	593	2.8	4.3 (4.4)	288	4.4	5.0 (5.1)	209	5.2	5.0 (5.2)
32–34	33.0	420	3.5	4.7 (4.8)	194	6.0	6.7 (6.8)	162	6.5	6.4 (6.5)
34–36	35.0	314	3.8	4.6 (4.6)	158	5.8	5.9 (6.0)	112	7.1	5.7 (5.8)
36–38	37.0	209	4.8	4.5 (4.6)	123	6.5	4.6 (4.7)	92	7.5	4.6 (4.7)
38–40	39.0	157	5.4	4.2 (4.2)	86	7.8	4.4 (4.6)	61	9.5	4.6 (4.7)
40–43	41.4	114	5.0	4.0 (4.1)	61	7.6	4.3 (4.4)	42	9.3	4.4 (4.6)
43–46	44.4	76	6.3	5.8 (5.8)	36	10.0	9.5 (9.5)	39	9.4	7.8 (7.9)
46–50	47.9	49	6.6	4.2 (4.2)	27	9.6	4.8 (4.9)	22	10.9	5.1 (5.3)
50–55	52.4	24	9.2	5.9 (5.8)	17	10.9	4.8 (4.9)	12	13.6	4.4 (4.6)
55–60	57.4	15	11.0	6.3 (6.2)	9.8	14.8	5.0 (5.1)	8.5	15.5	4.6 (4.8)
60–70	64.6	9.2	10.1	6.6 (6.5)	4.7	15.7	7.3 (7.3)	4.9	14.8	6.0 (6.1)
70–100	82.0	2.3	12.6	11.9 (11.8)	1.2	17.6	8.9 (8.9)	1.0	19.1	7.3 (7.2)

Table A.2: The p_T bin width, the weighted mean p_T within a bin, and the differential cross section times the dimuon branching fraction: $(\mathrm{d}\sigma/p_T)\mathcal{B}(\mathrm{Y}(n\mathrm{S}) \to \mu^+\mu^-)$ for the Y(1S), Y(2S), and Y(3S) with $0.6 < |y| < 1.2$. The notation is the same as for Table A.1.

p_T	$\langle p_T \rangle$	Y(1S) $\frac{\mathrm{d}\sigma}{\mathrm{d}p_T}\mathcal{B}$	$\frac{\sigma_{\text{stat}}}{\mathrm{d}\sigma/\mathrm{d}p_T}$	$\frac{\sigma_{\text{syst}}}{\mathrm{d}\sigma/\mathrm{d}p_T}$	Y(2S) $\frac{\mathrm{d}\sigma}{\mathrm{d}p_T}\mathcal{B}$	$\frac{\sigma_{\text{stat}}}{\mathrm{d}\sigma/\mathrm{d}p_T}$	$\frac{\sigma_{\text{syst}}}{\mathrm{d}\sigma/\mathrm{d}p_T}$	Y(3S) $\frac{\mathrm{d}\sigma}{\mathrm{d}p_T}\mathcal{B}$	$\frac{\sigma_{\text{stat}}}{\mathrm{d}\sigma/\mathrm{d}p_T}$	$\frac{\sigma_{\text{syst}}}{\mathrm{d}\sigma/\mathrm{d}p_T}$
GeV	GeV	(fb/GeV)	(%)	(%)	(fb/GeV)	(%)	(%)	(fb/GeV)	(%)	(%)
10–12	11.0	55260	0.5	6.1 (6.3)	18371	1.2	7.8 (8.2)	9855	1.6	8.9 (10.0)
12–14	13.0	31331	0.6	4.1 (4.2)	10973	1.1	4.9 (5.2)	6741	1.5	5.5 (6.0)
14–16	15.0	18063	0.7	3.8 (4.0)	6685	1.5	4.6 (4.8)	4298	2.0	5.5 (5.7)
16–18	17.0	10481	0.9	3.8 (3.9)	4105	1.7	4.9 (5.1)	2759	2.3	4.8 (5.0)
18–20	19.0	6286	1.1	3.7 (3.8)	2624	2.1	4.6 (4.8)	1871	2.6	4.6 (4.7)
20–22	21.0	3875	1.4	3.8 (3.9)	1746	2.4	4.7 (4.8)	1220	3.0	5.0 (5.2)
22–24	23.0	2439	1.6	3.6 (3.7)	1188	2.4	3.8 (3.9)	819	3.0	4.0 (4.2)
24–26	25.0	1633	1.9	3.8 (3.9)	865	2.8	4.0 (4.1)	530	3.7	4.0 (4.2)
26–28	27.0	1080	2.2	3.8 (3.9)	551	3.4	4.5 (4.5)	377	4.3	4.7 (4.8)
28–30	29.0	765	2.5	3.7 (3.8)	397	3.9	3.9 (4.0)	274	5.0	4.2 (4.3)
30–32	31.0	484	3.8	5.0 (5.1)	229	6.5	9.0 (9.0)	170	7.8	10.3 (10.3)
32–34	33.0	371	3.7	6.0 (6.1)	175	6.0	9.8 (9.8)	123	7.8	10.3 (10.4)
34–36	35.0	263	4.3	3.7 (3.8)	151	6.1	4.0 (4.1)	101	8.1	4.3 (4.4)
36–38	37.0	193	4.9	3.6 (3.7)	113	7.0	3.9 (4.0)	84	8.6	4.3 (4.4)
38–40	39.0	152	5.7	3.7 (3.8)	87	8.1	4.0 (4.1)	47	11.9	4.2 (4.3)
40–43	41.4	98	6.0	5.0 (5.0)	55	8.4	4.3 (4.4)	43	9.8	4.2 (4.3)
43–46	44.4	73	6.5	7.1 (7.1)	37	10.3	9.9 (9.9)	34	11.1	13.4 (13.4)
46–50	47.9	51	6.7	4.0 (4.0)	23	11.0	3.9 (4.0)	16	14.2	4.0 (4.2)
50–55	52.4	27	8.6	5.1 (5.1)	14	13.2	4.5 (4.5)	8.7	18.3	4.0 (4.2)
55–60	57.4	15	11.2	5.1 (5.0)	9.2	15.5	4.6 (4.6)	11	13.7	4.5 (4.7)
60–70	64.6	8.1	10.8	5.6 (5.6)	3.6	19.7	5.1 (5.1)	3.3	20.9	5.2 (5.3)
70–100	82.0	1.6	15.0	7.4 (7.2)	1.0	24.0	7.0 (6.9)	1.3	19.8	6.6 (6.7)

Table A.3: The p_T bin width, the weighted mean p_T within a bin, and the differential cross section times the dimuon branching fraction: $(d\sigma/p_T)\mathcal{B}(Y(nS) \to \mu^+\mu^-)$ for the Y(1S), Y(2S), and Y(3S) with $0 < |y| < 1.2$. The notation is the same as for Table A.1.

		Y(1S)			Y(2S)			Y(3S)		
p_T	$\langle p_T \rangle$	$\frac{d\sigma}{dp_T}\mathcal{B}$	$\frac{\sigma_{stat}}{d\sigma/dp_T}$	$\frac{\sigma_{syst}}{d\sigma/dp_T}$	$\frac{d\sigma}{dp_T}\mathcal{B}$	$\frac{\sigma_{stat}}{d\sigma/dp_T}$	$\frac{\sigma_{syst}}{d\sigma/dp_T}$	$\frac{d\sigma}{dp_T}\mathcal{B}$	$\frac{\sigma_{stat}}{d\sigma/dp_T}$	$\frac{\sigma_{syst}}{d\sigma/dp_T}$
GeV	GeV	(fb/GeV)	(%)	(%)	(fb/GeV)	(%)	(%)	(fb/GeV)	(%)	(%)
10–12	11.0	116415	0.4	6.4 (6.7)	38540	0.7	8.1 (8.7)	20882	1.1	9.3 (10.5)
12–14	13.0	65266	0.4	4.6 (4.9)	23088	0.8	5.4 (5.9)	13947	1.0	6.2 (6.9)
14–16	15.0	37778	0.5	4.3 (4.6)	14321	0.9	4.7 (5.1)	8909	1.3	5.2 (5.7)
16–18	17.0	22008	0.6	4.1 (4.4)	8969	1.1	4.7 (5.0)	5873	1.4	5.0 (5.3)
18–20	19.0	13212	0.7	4.1 (4.2)	5665	1.3	4.6 (4.8)	3842	1.6	4.7 (5.0)
20–22	21.0	8116	0.9	4.0 (4.1)	3683	1.5	4.4 (4.6)	2648	1.8	4.7 (4.9)
22–24	23.0	5162	1.0	3.9 (4.0)	2393	1.7	4.1 (4.2)	1713	2.0	4.3 (4.5)
24–26	25.0	3483	1.3	3.9 (4.0)	1715	1.9	4.2 (4.3)	1124	2.4	4.4 (4.5)
26–28	27.0	2197	1.5	4.0 (4.0)	1089	2.5	4.6 (4.7)	759	3.1	4.9 (5.0)
28–30	29.0	1611	1.8	4.0 (4.1)	811	2.8	4.6 (4.7)	588	3.4	4.8 (5.0)
30–32	31.0	1077	2.3	4.2 (4.3)	517	3.8	5.7 (5.7)	380	4.5	6.2 (6.3)
32–34	33.0	791	2.5	4.7 (4.7)	369	4.2	6.5 (6.6)	286	5.0	6.5 (6.6)
34–36	35.0	577	2.8	4.1 (4.1)	309	4.2	4.7 (4.7)	213	5.3	4.8 (4.9)
36–38	37.0	402	3.4	4.0 (4.1)	236	4.8	4.2 (4.3)	176	5.7	4.4 (4.6)
38–40	39.0	308	3.9	3.9 (3.9)	173	5.6	4.2 (4.3)	109	7.5	4.4 (4.5)
40–43	41.4	212	3.9	4.1 (4.2)	116	5.6	4.2 (4.3)	86	6.8	4.3 (4.5)
43–46	44.4	148	4.5	5.3 (5.3)	73	7.2	7.5 (7.5)	73	7.2	8.1 (8.2)
46–50	47.9	100	4.7	4.0 (4.0)	50	7.3	4.2 (4.3)	38	8.7	4.5 (4.6)
50–55	52.4	51	6.3	5.0 (5.0)	31	8.4	4.5 (4.6)	21	11.0	4.2 (4.4)
55–60	57.4	29	7.9	5.4 (5.4)	19	10.7	4.8 (4.8)	20	10.3	4.6 (4.7)
60–70	64.6	17	7.4	6.0 (5.9)	8.3	12.4	6.1 (6.1)	8.1	12.2	5.5 (5.6)
70–100	82.0	3.9	9.7	8.9 (8.8)	2.2	14.6	7.6 (7.5)	2.3	14.0	6.9 (6.9)

Table A.4: The p_T bin width and corrected yield ratios R_{21} and R_{31} for $|y| < 0.6$. The statistical uncertainty in the corrected yield ratios is given as the percentage of the ratio in the format: σ_{stat}/R_{n1} (%) ($n = 2,3$) and similarly for the systematic uncertainty. The statistical uncertainties are derived from the fit to the dimuon mass spectrum. The systematic uncertainties are discussed in the text. The 2.2% systematic uncertainty in the integrated luminosity is not included.

p_T	R_{21}	$\frac{\sigma_{stat}}{R_{21}}$	$\frac{\sigma_{syst}}{R_{21}}$	R_{31}	$\frac{\sigma_{stat}}{R_{31}}$	$\frac{\sigma_{syst}}{R_{31}}$
GeV		(%)	(%)		(%)	(%)
10–12	0.33	1.0	7.2	0.18	1.4	8.6
12–14	0.36	1.1	5.9	0.21	1.5	6.7
14–16	0.39	1.3	4.9	0.23	1.7	5.5
16–18	0.42	1.4	4.7	0.27	1.8	5.2
18–20	0.44	1.7	4.1	0.28	2.1	4.6
20–22	0.46	2.1	3.8	0.34	2.4	4.2
22–24	0.44	2.6	3.4	0.33	3.0	3.8
24–26	0.46	3.0	3.4	0.32	3.6	3.8
26–28	0.48	3.9	3.9	0.34	4.6	4.5
28–30	0.49	4.4	3.8	0.37	5.0	4.1
30–32	0.49	5.1	3.5	0.35	5.8	3.6
32–34	0.46	6.4	4.1	0.39	6.9	4.1
34–36	0.50	6.8	3.6	0.36	7.8	3.7
36–38	0.59	7.8	3.3	0.44	8.6	4.0
38–40	0.55	9.2	3.1	0.39	10.6	3.5
40–43	0.54	8.8	3.0	0.37	10.3	3.3
43–46	0.48	11.4	5.3	0.51	10.9	3.9
46–50	0.55	11.3	3.1	0.45	12.3	3.5
50–55	0.72	13.4	3.2	0.51	15.6	4.6
55–60	0.66	17.4	2.9	0.57	18.2	4.8
60–70	0.51	17.8	2.5	0.53	16.9	2.8
70–100	0.53	20.3	4.1	0.44	21.9	9.1

Table A.5: The p_T bin width and corrected yield ratios R_{21} and R_{31} for $0.6 < |y| < 1.2$. The notation is the same as for Table A.4.

p_T GeV	R_{21}	$\frac{\sigma_{\text{stat}}}{R_{21}}$ (%)	$\frac{\sigma_{\text{syst}}}{R_{21}}$ (%)	R_{31}	$\frac{\sigma_{\text{stat}}}{R_{31}}$ (%)	$\frac{\sigma_{\text{syst}}}{R_{31}}$ (%)
10–12	0.33	1.1	5.5	0.18	1.6	6.4
12–14	0.35	1.2	3.9	0.22	1.5	4.3
14–16	0.37	1.4	3.6	0.24	1.9	4.1
16–18	0.39	1.7	3.4	0.26	2.2	4.1
18–20	0.42	2.1	3.4	0.30	2.5	3.6
20–22	0.45	2.4	3.2	0.31	3.0	3.8
22–24	0.49	2.8	2.8	0.34	3.3	3.0
24–26	0.53	3.2	2.8	0.32	4.0	3.3
26–28	0.51	3.9	3.1	0.35	4.7	3.2
28–30	0.52	4.6	2.9	0.36	5.5	3.4
30–32	0.47	6.4	5.3	0.35	7.6	6.6
32–34	0.47	6.8	5.3	0.33	8.2	5.9
34–36	0.58	7.3	3.0	0.39	8.9	3.5
36–38	0.58	8.2	2.9	0.44	9.5	3.4
38–40	0.57	9.4	2.9	0.31	12.8	3.2
40–43	0.56	9.8	3.0	0.44	11.0	4.5
43–46	0.51	12.9	6.8	0.47	15.5	5.4
46–50	0.45	12.3	2.6	0.31	15.0	3.3
50–55	0.51	14.9	2.6	0.33	19.4	4.2
55–60	0.63	18.4	4.6	0.77	16.6	2.9
60–70	0.46	21.0	4.7	0.38	23.2	6.4
70–100	0.66	25.8	4.2	0.75	23.4	9.7

Table A.6: The p_T bin width and corrected yield ratios R_{21} and R_{31} for $|y| < 1.2$. The notation is the same as for Table A.4.

p_T GeV	R_{21}	$\frac{\sigma_{stat}}{R_{21}}$ (%)	$\frac{\sigma_{syst}}{R_{21}}$ (%)	R_{31}	$\frac{\sigma_{stat}}{R_{31}}$ (%)	$\frac{\sigma_{syst}}{R_{31}}$ (%)
10–12	0.33	0.7	6.2	0.18	1.0	7.4
12–14	0.35	0.8	4.8	0.21	1.1	5.4
14–16	0.38	1.0	4.1	0.24	1.3	4.5
16–18	0.41	1.1	4.0	0.27	1.4	4.3
18–20	0.43	1.3	3.6	0.29	1.6	3.9
20–22	0.45	1.6	3.4	0.33	1.9	3.7
22–24	0.46	1.9	3.0	0.33	2.2	3.3
24–26	0.49	2.2	3.0	0.32	2.7	3.4
26–28	0.50	2.8	3.2	0.34	3.3	3.4
28–30	0.50	3.2	3.1	0.36	3.7	3.5
30–32	0.48	4.0	3.3	0.35	4.6	3.5
32–34	0.47	4.7	3.8	0.36	5.3	4.0
34–36	0.53	5.0	3.1	0.37	5.9	3.5
36–38	0.58	5.7	3.1	0.44	6.4	3.4
38–40	0.56	6.6	3.0	0.35	8.2	3.3
40–43	0.55	6.6	2.9	0.40	7.5	3.2
43–46	0.49	8.6	4.5	0.50	8.9	3.7
46–50	0.49	8.4	2.7	0.37	9.7	3.2
50–55	0.59	10.1	2.6	0.40	12.5	3.6
55–60	0.65	12.6	2.8	0.65	12.4	3.0
60–70	0.49	13.6	2.5	0.45	13.9	2.6
70–100	0.56	16.0	3.3	0.50	16.5	7.0

Table A.7: The dimuon acceptance $\mathcal{A}$ calculated using the CMS measured polarization and its positive and negative uncertainties $\mathcal{A}(\sigma^{\pm})$, and the values of the acceptance assuming no polarization $\mathcal{A}(\mathrm{unpol})$, transverse polarization $\mathcal{A}(T)$, and longitudinal polarization $\mathcal{A}(L)$ for the $\Upsilon(1S)$ state and $|y| < 0.6$.

p_{T} [GeV]	$\mathcal{A}$	$\mathcal{A}(\sigma^+)$	$\mathcal{A}(\sigma^-)$	$\mathcal{A}(\mathrm{unpol})$	$\mathcal{A}(T)$	$\mathcal{A}(L)$
10–12	0.31	0.29	0.32	0.32	0.26	0.45
12–14	0.38	0.36	0.40	0.39	0.32	0.54
14–16	0.44	0.42	0.45	0.45	0.36	0.61
16–18	0.49	0.48	0.51	0.50	0.41	0.67
18–20	0.53	0.52	0.55	0.54	0.45	0.71
20–22	0.57	0.56	0.58	0.57	0.48	0.74
22–24	0.60	0.59	0.61	0.60	0.51	0.77
24–26	0.62	0.61	0.64	0.62	0.54	0.79
26–28	0.64	0.63	0.66	0.65	0.56	0.81
28–30	0.66	0.64	0.67	0.66	0.58	0.83
30–32	0.67	0.66	0.69	0.68	0.60	0.84
32–34	0.69	0.67	0.70	0.69	0.62	0.85
34–36	0.70	0.69	0.71	0.71	0.63	0.86
36–38	0.71	0.70	0.72	0.72	0.64	0.87
38–40	0.72	0.71	0.74	0.73	0.66	0.88
40–43	0.73	0.72	0.75	0.74	0.67	0.89
43–46	0.75	0.73	0.76	0.76	0.69	0.89
46–50	0.76	0.75	0.78	0.77	0.71	0.90
50–55	0.78	0.77	0.80	0.79	0.73	0.91
55–60	0.80	0.78	0.81	0.80	0.75	0.92
60–70	0.82	0.81	0.83	0.82	0.77	0.93
70–100	0.87	0.86	0.88	0.87	0.83	0.96

Table A.8: The dimuon acceptance $\mathcal{A}$ calculated using the CMS measured polarization and its positive and negative uncertainties $\mathcal{A}(\sigma^{\pm})$, and the values of the acceptance assuming no polarization $\mathcal{A}$(unpol), transverse polarization $\mathcal{A}(T)$, and longitudinal polarization $\mathcal{A}(L)$ for the Y(1S) state and $0.6 < |y| < 1.2$.

p_{T} [GeV]	$\mathcal{A}$	$\mathcal{A}(\sigma^{+})$	$\mathcal{A}(\sigma^{-})$	$\mathcal{A}$(unpol)	$\mathcal{A}(T)$	$\mathcal{A}(L)$
10–12	0.29	0.28	0.30	0.29	0.24	0.38
12–14	0.35	0.34	0.36	0.35	0.30	0.46
14–16	0.42	0.41	0.43	0.42	0.36	0.54
16–18	0.47	0.46	0.48	0.47	0.40	0.60
18–20	0.52	0.51	0.53	0.51	0.44	0.66
20–22	0.55	0.54	0.56	0.55	0.48	0.70
22–24	0.59	0.58	0.60	0.59	0.51	0.74
24–26	0.61	0.60	0.63	0.62	0.54	0.77
26–28	0.64	0.63	0.65	0.64	0.57	0.79
28–30	0.66	0.64	0.67	0.66	0.59	0.81
30–32	0.67	0.66	0.69	0.68	0.61	0.83
32–34	0.69	0.67	0.70	0.70	0.63	0.84
34–36	0.70	0.69	0.71	0.71	0.64	0.86
36–38	0.71	0.70	0.72	0.73	0.66	0.87
38–40	0.72	0.71	0.74	0.74	0.67	0.88
40–43	0.74	0.73	0.75	0.75	0.68	0.88
43–46	0.75	0.74	0.77	0.77	0.70	0.89
46–50	0.77	0.76	0.78	0.78	0.72	0.90
50–55	0.79	0.78	0.80	0.80	0.74	0.91
55–60	0.81	0.80	0.82	0.81	0.76	0.92
60–70	0.83	0.82	0.84	0.83	0.78	0.93
70–100	0.88	0.87	0.89	0.88	0.84	0.96

Table A.9: The dimuon acceptance $\mathcal{A}$ calculated using the CMS measured polarization and its positive and negative uncertainties $\mathcal{A}(\sigma^{\pm})$, and the values of the acceptance assuming no polarization $\mathcal{A}$(unpol), transverse polarization $\mathcal{A}(T)$, and longitudinal polarization $\mathcal{A}(L)$ for the Y(1S) state and $|y| < 1.2$.

p_{T} [GeV]	$\mathcal{A}$	$\mathcal{A}(\sigma^{+})$	$\mathcal{A}(\sigma^{-})$	$\mathcal{A}$(unpol)	$\mathcal{A}(T)$	$\mathcal{A}(L)$
10–12	0.30	0.28	0.31	0.30	0.25	0.42
12–14	0.37	0.35	0.38	0.37	0.31	0.50
14–16	0.43	0.42	0.44	0.43	0.36	0.57
16–18	0.48	0.47	0.49	0.48	0.41	0.64
18–20	0.52	0.51	0.54	0.53	0.45	0.68
20–22	0.56	0.55	0.57	0.56	0.48	0.72
22–24	0.59	0.58	0.61	0.59	0.51	0.75
24–26	0.62	0.61	0.63	0.62	0.54	0.78
26–28	0.64	0.63	0.65	0.64	0.56	0.80
28–30	0.66	0.64	0.67	0.66	0.58	0.82
30–32	0.67	0.66	0.69	0.68	0.60	0.84
32–34	0.69	0.67	0.70	0.70	0.62	0.85
34–36	0.70	0.69	0.71	0.71	0.64	0.86
36–38	0.71	0.70	0.72	0.72	0.65	0.87
38–40	0.72	0.71	0.74	0.73	0.66	0.88
40–43	0.74	0.72	0.75	0.75	0.68	0.88
43–46	0.75	0.74	0.77	0.76	0.70	0.89
46–50	0.77	0.76	0.78	0.78	0.71	0.90
50–55	0.79	0.77	0.80	0.79	0.73	0.91
55–60	0.80	0.79	0.81	0.81	0.75	0.92
60–70	0.82	0.81	0.84	0.83	0.78	0.93
70–100	0.87	0.86	0.89	0.88	0.83	0.96

Table A.10: The dimuon acceptance $\mathcal{A}$ calculated using the CMS measured polarization and its positive and negative uncertainties $\mathcal{A}(\sigma^{\pm})$, and the values of the acceptance assuming no polarization $\mathcal{A}(\text{unpol})$, transverse polarization $\mathcal{A}(T)$, and longitudinal polarization $\mathcal{A}(L)$ for the Y(2S) state and $|y| < 0.6$.

p_{T} [GeV]	$\mathcal{A}$	$\mathcal{A}(\sigma^{+})$	$\mathcal{A}(\sigma^{-})$	$\mathcal{A}(\text{unpol})$	$\mathcal{A}(T)$	$\mathcal{A}(L)$
10–12	0.31	0.30	0.33	0.34	0.27	0.48
12–14	0.37	0.36	0.39	0.41	0.33	0.56
14–16	0.43	0.41	0.45	0.47	0.38	0.63
16–18	0.48	0.46	0.50	0.51	0.42	0.68
18–20	0.52	0.51	0.54	0.55	0.46	0.73
20–22	0.56	0.54	0.57	0.58	0.49	0.76
22–24	0.59	0.57	0.61	0.61	0.52	0.79
24–26	0.61	0.59	0.63	0.63	0.55	0.81
26–28	0.64	0.62	0.65	0.66	0.58	0.83
28–30	0.65	0.63	0.67	0.67	0.59	0.84
30–32	0.66	0.64	0.68	0.69	0.61	0.85
32–34	0.68	0.66	0.70	0.71	0.63	0.87
34–36	0.69	0.67	0.71	0.72	0.64	0.88
36–38	0.70	0.68	0.72	0.73	0.65	0.88
38–40	0.71	0.69	0.73	0.74	0.66	0.89
40–43	0.73	0.71	0.75	0.76	0.69	0.90
43–46	0.74	0.72	0.76	0.77	0.70	0.91
46–50	0.76	0.74	0.78	0.79	0.72	0.92
50–55	0.77	0.76	0.79	0.80	0.74	0.92
55–60	0.79	0.78	0.81	0.82	0.76	0.93
60–70	0.82	0.80	0.83	0.84	0.78	0.95
70–100	0.87	0.85	0.88	0.88	0.84	0.97

Table A.11: The dimuon acceptance $\mathcal{A}$ calculated using the CMS measured polarization and its positive and negative uncertainties $\mathcal{A}(\sigma^{\pm})$, and the values of the acceptance assuming no polarization $\mathcal{A}(\text{unpol})$, transverse polarization $\mathcal{A}(T)$, and longitudinal polarization $\mathcal{A}(L)$ for the Y(2S) state and $0.6 < |y| < 1.2$.

p_T [GeV]	$\mathcal{A}$	$\mathcal{A}(\sigma^{+})$	$\mathcal{A}(\sigma^{-})$	$\mathcal{A}(\text{unpol})$	$\mathcal{A}(T)$	$\mathcal{A}(L)$
10–12	0.28	0.27	0.30	0.30	0.25	0.39
12–14	0.35	0.34	0.37	0.36	0.31	0.47
14–16	0.42	0.41	0.43	0.42	0.36	0.54
16–18	0.47	0.46	0.49	0.47	0.41	0.60
18–20	0.51	0.50	0.53	0.52	0.45	0.66
20–22	0.54	0.53	0.56	0.56	0.49	0.70
22–24	0.56	0.55	0.58	0.59	0.52	0.74
24–26	0.58	0.57	0.60	0.62	0.54	0.77
26–28	0.61	0.60	0.63	0.65	0.57	0.79
28–30	0.64	0.62	0.66	0.67	0.60	0.82
30–32	0.66	0.64	0.68	0.69	0.61	0.84
32–34	0.68	0.66	0.69	0.70	0.63	0.85
34–36	0.69	0.68	0.71	0.72	0.65	0.87
36–38	0.72	0.70	0.73	0.74	0.67	0.88
38–40	0.72	0.71	0.74	0.75	0.68	0.89
40–43	0.74	0.72	0.76	0.76	0.69	0.89
43–46	0.76	0.74	0.78	0.78	0.71	0.91
46–50	0.77	0.75	0.79	0.79	0.73	0.92
50–55	0.79	0.78	0.81	0.81	0.75	0.93
55–60	0.81	0.80	0.83	0.83	0.77	0.94
60–70	0.83	0.82	0.85	0.84	0.79	0.95
70–100	0.88	0.87	0.90	0.89	0.85	0.97

Table A.12: The dimuon acceptance $\mathcal{A}$ calculated using the CMS measured polarization and its positive and negative uncertainties $\mathcal{A}(\sigma^{\pm})$, and the values of the acceptance assuming no polarization $\mathcal{A}$(unpol), transverse polarization $\mathcal{A}(T)$, and longitudinal polarization $\mathcal{A}(L)$ for the Y(2S) state and $|y| < 1.2$.

p_{T} [GeV]	$\mathcal{A}$	$\mathcal{A}(\sigma^{+})$	$\mathcal{A}(\sigma^{-})$	$\mathcal{A}$(unpol)	$\mathcal{A}(T)$	$\mathcal{A}(L)$
10–12	0.30	0.28	0.32	0.32	0.26	0.44
12–14	0.36	0.35	0.38	0.38	0.32	0.52
14–16	0.42	0.41	0.44	0.44	0.37	0.59
16–18	0.47	0.46	0.49	0.49	0.41	0.64
18–20	0.52	0.50	0.53	0.53	0.46	0.69
20–22	0.55	0.53	0.56	0.57	0.49	0.73
22–24	0.58	0.56	0.59	0.60	0.52	0.76
24–26	0.60	0.58	0.61	0.62	0.54	0.79
26–28	0.62	0.61	0.64	0.65	0.57	0.81
28–30	0.64	0.63	0.66	0.67	0.59	0.83
30–32	0.66	0.64	0.68	0.69	0.61	0.85
32–34	0.68	0.66	0.70	0.71	0.63	0.86
34–36	0.69	0.67	0.71	0.72	0.65	0.87
36–38	0.71	0.69	0.72	0.73	0.66	0.88
38–40	0.71	0.70	0.73	0.74	0.67	0.89
40–43	0.73	0.72	0.75	0.76	0.69	0.90
43–46	0.75	0.73	0.77	0.77	0.71	0.91
46–50	0.76	0.75	0.78	0.79	0.72	0.92
50–55	0.78	0.77	0.80	0.80	0.74	0.93
55–60	0.80	0.79	0.82	0.82	0.76	0.93
60–70	0.82	0.81	0.84	0.84	0.79	0.95
70–100	0.87	0.86	0.89	0.88	0.84	0.97

Table A.13: The dimuon acceptance $\mathcal{A}$ calculated using the CMS measured polarization and its positive and negative uncertainties $\mathcal{A}(\sigma^{\pm})$, and the values of the acceptance assuming no polarization $\mathcal{A}$(unpol), transverse polarization $\mathcal{A}(T)$, and longitudinal polarization $\mathcal{A}(L)$ for the Y(3S) state and $|y| < 0.6$.

p_T [GeV]	$\mathcal{A}$	$\mathcal{A}(\sigma^+)$	$\mathcal{A}(\sigma^-)$	$\mathcal{A}$(unpol)	$\mathcal{A}(T)$	$\mathcal{A}(L)$
10–12	0.34	0.32	0.37	0.35	0.28	0.49
12–14	0.39	0.37	0.42	0.42	0.34	0.58
14–16	0.44	0.42	0.46	0.47	0.39	0.64
16–18	0.49	0.47	0.51	0.52	0.43	0.69
18–20	0.52	0.50	0.55	0.55	0.46	0.73
20–22	0.55	0.54	0.58	0.59	0.50	0.77
22–24	0.59	0.57	0.60	0.62	0.53	0.79
24–26	0.61	0.59	0.63	0.64	0.55	0.82
26–28	0.63	0.62	0.66	0.67	0.58	0.84
28–30	0.65	0.63	0.67	0.68	0.60	0.85
30–32	0.67	0.65	0.69	0.70	0.61	0.86
32–34	0.69	0.67	0.71	0.71	0.63	0.87
34–36	0.70	0.68	0.72	0.73	0.65	0.88
36–38	0.72	0.70	0.74	0.74	0.67	0.89
38–40	0.73	0.70	0.75	0.75	0.67	0.90
40–43	0.74	0.72	0.76	0.76	0.69	0.91
43–46	0.75	0.73	0.78	0.78	0.71	0.91
46–50	0.77	0.75	0.79	0.79	0.72	0.92
50–55	0.79	0.77	0.81	0.81	0.74	0.93
55–60	0.81	0.79	0.83	0.82	0.77	0.94
60–70	0.82	0.81	0.85	0.84	0.79	0.95
70–100	0.87	0.85	0.89	0.88	0.84	0.98

Table A.14: The dimuon acceptance $\mathcal{A}$ calculated using the CMS measured polarization and its positive and negative uncertainties $\mathcal{A}(\sigma^{\pm})$, and the values of the acceptance assuming no polarization $\mathcal{A}$(unpol), transverse polarization $\mathcal{A}(T)$, and longitudinal polarization $\mathcal{A}(L)$ for the Y(3S) state and $0.6 < |y| < 1.2$.

p_T [GeV]	$\mathcal{A}$	$\mathcal{A}(\sigma^+)$	$\mathcal{A}(\sigma^-)$	$\mathcal{A}$(unpol)	$\mathcal{A}(T)$	$\mathcal{A}(L)$
10–12	0.31	0.29	0.33	0.30	0.25	0.40
12–14	0.35	0.34	0.37	0.36	0.31	0.47
14–16	0.40	0.39	0.41	0.42	0.36	0.54
16–18	0.44	0.43	0.46	0.48	0.41	0.60
18–20	0.49	0.48	0.50	0.52	0.46	0.66
20–22	0.53	0.52	0.55	0.56	0.49	0.70
22–24	0.58	0.56	0.59	0.59	0.52	0.73
24–26	0.61	0.60	0.63	0.62	0.55	0.77
26–28	0.63	0.61	0.65	0.64	0.57	0.79
28–30	0.65	0.63	0.67	0.67	0.60	0.82
30–32	0.66	0.65	0.68	0.69	0.62	0.84
32–34	0.68	0.66	0.70	0.71	0.64	0.85
34–36	0.69	0.67	0.71	0.72	0.65	0.87
36–38	0.70	0.68	0.72	0.74	0.67	0.88
38–40	0.72	0.70	0.74	0.76	0.69	0.89
40–43	0.73	0.72	0.76	0.77	0.70	0.90
43–46	0.75	0.73	0.77	0.78	0.72	0.91
46–50	0.77	0.75	0.79	0.80	0.73	0.92
50–55	0.79	0.77	0.81	0.81	0.75	0.93
55–60	0.81	0.79	0.83	0.83	0.77	0.94
60–70	0.83	0.82	0.85	0.85	0.80	0.95
70–100	0.88	0.87	0.90	0.89	0.85	0.98

Table A.15: The dimuon acceptance $\mathcal{A}$ calculated using the CMS measured polarization and its positive and negative uncertainties $\mathcal{A}(\sigma^{\pm})$, and the values of the acceptance assuming no polarization $\mathcal{A}(\text{unpol})$, transverse polarization $\mathcal{A}(T)$, and longitudinal polarization $\mathcal{A}(L)$ for the Y(3S) state and $|y| < 1.2$.

p_T [GeV]	$\mathcal{A}$	$\mathcal{A}(\sigma^+)$	$\mathcal{A}(\sigma^-)$	$\mathcal{A}(\text{unpol})$	$\mathcal{A}(T)$	$\mathcal{A}(L)$
10–12	0.32	0.30	0.35	0.33	0.27	0.44
12–14	0.37	0.36	0.39	0.39	0.33	0.52
14–16	0.42	0.40	0.44	0.45	0.37	0.59
16–18	0.47	0.45	0.48	0.50	0.42	0.65
18–20	0.51	0.49	0.52	0.54	0.46	0.69
20–22	0.54	0.53	0.56	0.57	0.49	0.73
22–24	0.58	0.57	0.60	0.60	0.53	0.76
24–26	0.61	0.59	0.63	0.63	0.55	0.79
26–28	0.63	0.61	0.65	0.65	0.58	0.81
28–30	0.65	0.63	0.67	0.68	0.60	0.83
30–32	0.67	0.65	0.69	0.69	0.62	0.85
32–34	0.68	0.66	0.70	0.71	0.63	0.86
34–36	0.69	0.67	0.72	0.72	0.65	0.87
36–38	0.71	0.69	0.73	0.74	0.67	0.89
38–40	0.72	0.70	0.75	0.75	0.68	0.89
40–43	0.74	0.72	0.76	0.77	0.70	0.90
43–46	0.75	0.73	0.77	0.78	0.71	0.91
46–50	0.77	0.75	0.79	0.79	0.73	0.92
50–55	0.79	0.77	0.81	0.81	0.75	0.93
55–60	0.81	0.79	0.83	0.83	0.77	0.94
60–70	0.83	0.81	0.85	0.85	0.79	0.95
70–100	0.88	0.86	0.90	0.89	0.84	0.98

B The CMS Collaboration

Yerevan Physics Institute, Yerevan, Armenia
V. Khachatryan, A.M. Sirunyan, A. Tumasyan

Institut für Hochenergiephysik der OeAW, Wien, Austria
W. Adam, T. Bergauer, M. Dragicevic, J. Erö, M. Friedl, R. Frühwirth[1], V.M. Ghete, C. Hartl, N. Hörmann, J. Hrubec, M. Jeitler[1], W. Kiesenhofer, V. Knünz, M. Krammer[1], I. Krätschmer, D. Liko, I. Mikulec, D. Rabady[2], B. Rahbaran, H. Rohringer, R. Schöfbeck, J. Strauss, W. Treberer-Treberspurg, W. Waltenberger, C.-E. Wulz[1]

National Centre for Particle and High Energy Physics, Minsk, Belarus
V. Mossolov, N. Shumeiko, J. Suarez Gonzalez

Universiteit Antwerpen, Antwerpen, Belgium
S. Alderweireldt, S. Bansal, T. Cornelis, E.A. De Wolf, X. Janssen, A. Knutsson, J. Lauwers, S. Luyckx, S. Ochesanu, R. Rougny, M. Van De Klundert, H. Van Haevermaet, P. Van Mechelen, N. Van Remortel, A. Van Spilbeeck

Vrije Universiteit Brussel, Brussel, Belgium
F. Blekman, S. Blyweert, J. D'Hondt, N. Daci, N. Heracleous, J. Keaveney, S. Lowette, M. Maes, A. Olbrechts, Q. Python, D. Strom, S. Tavernier, W. Van Doninck, P. Van Mulders, G.P. Van Onsem, I. Villella

Université Libre de Bruxelles, Bruxelles, Belgium
C. Caillol, B. Clerbaux, G. De Lentdecker, D. Dobur, L. Favart, A.P.R. Gay, A. Grebenyuk, A. Léonard, A. Mohammadi, L. Perniè[2], A. Randle-conde, T. Reis, T. Seva, L. Thomas, C. Vander Velde, P. Vanlaer, J. Wang, F. Zenoni

Ghent University, Ghent, Belgium
V. Adler, K. Beernaert, L. Benucci, A. Cimmino, S. Costantini, S. Crucy, S. Dildick, A. Fagot, G. Garcia, J. Mccartin, A.A. Ocampo Rios, D. Poyraz, D. Ryckbosch, S. Salva Diblen, M. Sigamani, N. Strobbe, F. Thyssen, M. Tytgat, E. Yazgan, N. Zaganidis

Université Catholique de Louvain, Louvain-la-Neuve, Belgium
S. Basegmez, C. Beluffi[3], G. Bruno, R. Castello, A. Caudron, L. Ceard, G.G. Da Silveira, C. Delaere, T. du Pree, D. Favart, L. Forthomme, A. Giammanco[4], J. Hollar, A. Jafari, P. Jez, M. Komm, V. Lemaitre, C. Nuttens, L. Perrini, A. Pin, K. Piotrzkowski, A. Popov[5], L. Quertenmont, M. Selvaggi, M. Vidal Marono, J.M. Vizan Garcia

Université de Mons, Mons, Belgium
N. Beliy, T. Caebergs, E. Daubie, G.H. Hammad

Centro Brasileiro de Pesquisas Fisicas, Rio de Janeiro, Brazil
W.L. Aldá Júnior, G.A. Alves, L. Brito, M. Correa Martins Junior, T. Dos Reis Martins, J. Molina, C. Mora Herrera, M.E. Pol, P. Rebello Teles

Universidade do Estado do Rio de Janeiro, Rio de Janeiro, Brazil
W. Carvalho, J. Chinellato[6], A. Custódio, E.M. Da Costa, D. De Jesus Damiao, C. De Oliveira Martins, S. Fonseca De Souza, H. Malbouisson, D. Matos Figueiredo, L. Mundim, H. Nogima, W.L. Prado Da Silva, J. Santaolalla, A. Santoro, A. Sznajder, E.J. Tonelli Manganote[6], A. Vilela Pereira

Universidade Estadual Paulista [a]**, Universidade Federal do ABC** [b]**, São Paulo, Brazil**
C.A. Bernardes[b], S. Dogra[a], T.R. Fernandez Perez Tomei[a], E.M. Gregores[b], P.G. Mercadante[b], S.F. Novaes[a], Sandra S. Padula[a]

Institute for Nuclear Research and Nuclear Energy, Sofia, Bulgaria
A. Aleksandrov, V. Genchev[2], R. Hadjiiska, P. Iaydjiev, A. Marinov, S. Piperov, M. Rodozov, S. Stoykova, G. Sultanov, M. Vutova

University of Sofia, Sofia, Bulgaria
A. Dimitrov, I. Glushkov, L. Litov, B. Pavlov, P. Petkov

Institute of High Energy Physics, Beijing, China
J.G. Bian, G.M. Chen, H.S. Chen, M. Chen, T. Cheng, R. Du, C.H. Jiang, R. Plestina[7], F. Romeo, J. Tao, Z. Wang

State Key Laboratory of Nuclear Physics and Technology, Peking University, Beijing, China
C. Asawatangtrakuldee, Y. Ban, S. Liu, Y. Mao, S.J. Qian, D. Wang, Z. Xu, L. Zhang, W. Zou

Universidad de Los Andes, Bogota, Colombia
C. Avila, A. Cabrera, L.F. Chaparro Sierra, C. Florez, J.P. Gomez, B. Gomez Moreno, J.C. Sanabria

University of Split, Faculty of Electrical Engineering, Mechanical Engineering and Naval Architecture, Split, Croatia
N. Godinovic, D. Lelas, D. Polic, I. Puljak

University of Split, Faculty of Science, Split, Croatia
Z. Antunovic, M. Kovac

Institute Rudjer Boskovic, Zagreb, Croatia
V. Brigljevic, K. Kadija, J. Luetic, D. Mekterovic, L. Sudic

University of Cyprus, Nicosia, Cyprus
A. Attikis, G. Mavromanolakis, J. Mousa, C. Nicolaou, F. Ptochos, P.A. Razis, H. Rykaczewski

Charles University, Prague, Czech Republic
M. Bodlak, M. Finger, M. Finger Jr.[8]

Academy of Scientific Research and Technology of the Arab Republic of Egypt, Egyptian Network of High Energy Physics, Cairo, Egypt
Y. Assran[9], A. Ellithi Kamel[10], M.A. Mahmoud[11], A. Radi[12,13]

National Institute of Chemical Physics and Biophysics, Tallinn, Estonia
M. Kadastik, M. Murumaa, M. Raidal, A. Tiko

Department of Physics, University of Helsinki, Helsinki, Finland
P. Eerola, M. Voutilainen

Helsinki Institute of Physics, Helsinki, Finland
J. Härkönen, V. Karimäki, R. Kinnunen, M.J. Kortelainen, T. Lampén, K. Lassila-Perini, S. Lehti, T. Lindén, P. Luukka, T. Mäenpää, T. Peltola, E. Tuominen, J. Tuominiemi, E. Tuovinen, L. Wendland

Lappeenranta University of Technology, Lappeenranta, Finland
J. Talvitie, T. Tuuva

DSM/IRFU, CEA/Saclay, Gif-sur-Yvette, France
M. Besancon, F. Couderc, M. Dejardin, D. Denegri, B. Fabbro, J.L. Faure, C. Favaro, F. Ferri, S. Ganjour, A. Givernaud, P. Gras, G. Hamel de Monchenault, P. Jarry, E. Locci, J. Malcles, J. Rander, A. Rosowsky, M. Titov

Laboratoire Leprince-Ringuet, Ecole Polytechnique, IN2P3-CNRS, Palaiseau, France
S. Baffioni, F. Beaudette, P. Busson, E. Chapon, C. Charlot, T. Dahms, M. Dalchenko, L. Dobrzynski, N. Filipovic, A. Florent, R. Granier de Cassagnac, L. Mastrolorenzo, P. Miné, I.N. Naranjo, M. Nguyen, C. Ochando, G. Ortona, P. Paganini, S. Regnard, R. Salerno, J.B. Sauvan, Y. Sirois, C. Veelken, Y. Yilmaz, A. Zabi

Institut Pluridisciplinaire Hubert Curien, Université de Strasbourg, Université de Haute Alsace Mulhouse, CNRS/IN2P3, Strasbourg, France
J.-L. Agram[14], J. Andrea, A. Aubin, D. Bloch, J.-M. Brom, E.C. Chabert, C. Collard, E. Conte[14], J.-C. Fontaine[14], D. Gelé, U. Goerlach, C. Goetzmann, A.-C. Le Bihan, K. Skovpen, P. Van Hove

Centre de Calcul de l'Institut National de Physique Nucleaire et de Physique des Particules, CNRS/IN2P3, Villeurbanne, France
S. Gadrat

Université de Lyon, Université Claude Bernard Lyon 1, CNRS-IN2P3, Institut de Physique Nucléaire de Lyon, Villeurbanne, France
S. Beauceron, N. Beaupere, C. Bernet[7], G. Boudoul[2], E. Bouvier, S. Brochet, C.A. Carrillo Montoya, J. Chasserat, R. Chierici, D. Contardo[2], B. Courbon, P. Depasse, H. El Mamouni, J. Fan, J. Fay, S. Gascon, M. Gouzevitch, B. Ille, T. Kurca, M. Lethuillier, L. Mirabito, A.L. Pequegnot, S. Perries, J.D. Ruiz Alvarez, D. Sabes, L. Sgandurra, V. Sordini, M. Vander Donckt, P. Verdier, S. Viret, H. Xiao

Institute of High Energy Physics and Informatization, Tbilisi State University, Tbilisi, Georgia
I. Bagaturia[15]

RWTH Aachen University, I. Physikalisches Institut, Aachen, Germany
C. Autermann, S. Beranek, M. Bontenackels, M. Edelhoff, L. Feld, A. Heister, K. Klein, M. Lipinski, A. Ostapchuk, M. Preuten, F. Raupach, J. Sammet, S. Schael, J.F. Schulte, H. Weber, B. Wittmer, V. Zhukov[5]

RWTH Aachen University, III. Physikalisches Institut A, Aachen, Germany
M. Ata, M. Brodski, E. Dietz-Laursonn, D. Duchardt, M. Erdmann, R. Fischer, A. Güth, T. Hebbeker, C. Heidemann, K. Hoepfner, D. Klingebiel, S. Knutzen, P. Kreuzer, M. Merschmeyer, A. Meyer, P. Millet, M. Olschewski, K. Padeken, P. Papacz, H. Reithler, S.A. Schmitz, L. Sonnenschein, D. Teyssier, S. Thüer, M. Weber

RWTH Aachen University, III. Physikalisches Institut B, Aachen, Germany
V. Cherepanov, Y. Erdogan, G. Flügge, H. Geenen, M. Geisler, W. Haj Ahmad, F. Hoehle, B. Kargoll, T. Kress, Y. Kuessel, A. Künsken, J. Lingemann[2], A. Nowack, I.M. Nugent, O. Pooth, A. Stahl

Deutsches Elektronen-Synchrotron, Hamburg, Germany
M. Aldaya Martin, I. Asin, N. Bartosik, J. Behr, U. Behrens, A.J. Bell, A. Bethani, K. Borras, A. Burgmeier, A. Cakir, L. Calligaris, A. Campbell, S. Choudhury, F. Costanza, C. Diez Pardos, G. Dolinska, S. Dooling, T. Dorland, G. Eckerlin, D. Eckstein, T. Eichhorn, G. Flucke, J. Garay Garcia, A. Geiser, A. Gizhko, P. Gunnellini, J. Hauk, M. Hempel[16], H. Jung, A. Kalogeropoulos, O. Karacheban[16], M. Kasemann, P. Katsas, J. Kieseler, C. Kleinwort, I. Korol,

D. Krücker, W. Lange, J. Leonard, K. Lipka, A. Lobanov, W. Lohmann[16], B. Lutz, R. Mankel, I. Marfin[16], I.-A. Melzer-Pellmann, A.B. Meyer, G. Mittag, J. Mnich, A. Mussgiller, S. Naumann-Emme, A. Nayak, E. Ntomari, H. Perrey, D. Pitzl, R. Placakyte, A. Raspereza, P.M. Ribeiro Cipriano, B. Roland, E. Ron, M.Ö. Sahin, J. Salfeld-Nebgen, P. Saxena, T. Schoerner-Sadenius, M. Schröder, C. Seitz, S. Spannagel, A.D.R. Vargas Trevino, R. Walsh, C. Wissing

University of Hamburg, Hamburg, Germany
V. Blobel, M. Centis Vignali, A.R. Draeger, J. Erfle, E. Garutti, K. Goebel, M. Görner, J. Haller, M. Hoffmann, R.S. Höing, A. Junkes, H. Kirschenmann, R. Klanner, R. Kogler, T. Lapsien, T. Lenz, I. Marchesini, D. Marconi, J. Ott, T. Peiffer, A. Perieanu, N. Pietsch, J. Poehlsen, T. Poehlsen, D. Rathjens, C. Sander, H. Schettler, P. Schleper, E. Schlieckau, A. Schmidt, M. Seidel, V. Sola, H. Stadie, G. Steinbrück, D. Troendle, E. Usai, L. Vanelderen, A. Vanhoefer

Institut für Experimentelle Kernphysik, Karlsruhe, Germany
C. Barth, C. Baus, J. Berger, C. Böser, E. Butz, T. Chwalek, W. De Boer, A. Descroix, A. Dierlamm, M. Feindt, F. Frensch, M. Giffels, A. Gilbert, F. Hartmann[2], T. Hauth, U. Husemann, I. Katkov[5], A. Kornmayer[2], P. Lobelle Pardo, M.U. Mozer, T. Müller, Th. Müller, A. Nürnberg, G. Quast, K. Rabbertz, S. Röcker, H.J. Simonis, F.M. Stober, R. Ulrich, J. Wagner-Kuhr, S. Wayand, T. Weiler, R. Wolf

Institute of Nuclear and Particle Physics (INPP),   NCSR Demokritos, Aghia Paraskevi, Greece
G. Anagnostou, G. Daskalakis, T. Geralis, V.A. Giakoumopoulou, A. Kyriakis, D. Loukas, A. Markou, C. Markou, A. Psallidas, I. Topsis-Giotis

University of Athens, Athens, Greece
A. Agapitos, S. Kesisoglou, A. Panagiotou, N. Saoulidou, E. Stiliaris

University of Ioánnina, Ioánnina, Greece
X. Aslanoglou, I. Evangelou, G. Flouris, C. Foudas, P. Kokkas, N. Manthos, I. Papadopoulos, E. Paradas, J. Strologas

Wigner Research Centre for Physics, Budapest, Hungary
G. Bencze, C. Hajdu, P. Hidas, D. Horvath[17], F. Sikler, V. Veszpremi, G. Vesztergombi[18], A.J. Zsigmond

Institute of Nuclear Research ATOMKI, Debrecen, Hungary
N. Beni, S. Czellar, J. Karancsi[19], J. Molnar, J. Palinkas, Z. Szillasi

University of Debrecen, Debrecen, Hungary
A. Makovec, P. Raics, Z.L. Trocsanyi, B. Ujvari

National Institute of Science Education and Research, Bhubaneswar, India
S.K. Swain

Panjab University, Chandigarh, India
S.B. Beri, V. Bhatnagar, R. Gupta, U.Bhawandeep, A.K. Kalsi, M. Kaur, R. Kumar, M. Mittal, N. Nishu, J.B. Singh

University of Delhi, Delhi, India
Ashok Kumar, Arun Kumar, S. Ahuja, A. Bhardwaj, B.C. Choudhary, A. Kumar, S. Malhotra, M. Naimuddin, K. Ranjan, V. Sharma

Saha Institute of Nuclear Physics, Kolkata, India
S. Banerjee, S. Bhattacharya, K. Chatterjee, S. Dutta, B. Gomber, Sa. Jain, Sh. Jain, R. Khurana, A. Modak, S. Mukherjee, D. Roy, S. Sarkar, M. Sharan

Bhabha Atomic Research Centre, Mumbai, India
A. Abdulsalam, D. Dutta, V. Kumar, A.K. Mohanty[2], L.M. Pant, P. Shukla, A. Topkar

Tata Institute of Fundamental Research, Mumbai, India
T. Aziz, S. Banerjee, S. Bhowmik[20], R.M. Chatterjee, R.K. Dewanjee, S. Dugad, S. Ganguly, S. Ghosh, M. Guchait, A. Gurtu[21], G. Kole, S. Kumar, M. Maity[20], G. Majumder, K. Mazumdar, G.B. Mohanty, B. Parida, K. Sudhakar, N. Wickramage[22]

Indian Institute of Science Education and Research (IISER), Pune, India
S. Sharma

Institute for Research in Fundamental Sciences (IPM), Tehran, Iran
H. Bakhshiansohi, H. Behnamian, S.M. Etesami[23], A. Fahim[24], R. Goldouzian, M. Khakzad, M. Mohammadi Najafabadi, M. Naseri, S. Paktinat Mehdiabadi, F. Rezaei Hosseinabadi, B. Safarzadeh[25], M. Zeinali

University College Dublin, Dublin, Ireland
M. Felcini, M. Grunewald

INFN Sezione di Bari [a], Università di Bari [b], Politecnico di Bari [c], Bari, Italy
M. Abbrescia[a,b], C. Calabria[a,b], S.S. Chhibra[a,b], A. Colaleo[a], D. Creanza[a,c], L. Cristella[a,b], N. De Filippis[a,c], M. De Palma[a,b], L. Fiore[a], G. Iaselli[a,c], G. Maggi[a,c], M. Maggi[a], S. My[a,c], S. Nuzzo[a,b], A. Pompili[a,b], G. Pugliese[a,c], R. Radogna[a,b,2], G. Selvaggi[a,b], A. Sharma[a], L. Silvestris[a,2], R. Venditti[a,b], P. Verwilligen[a]

INFN Sezione di Bologna [a], Università di Bologna [b], Bologna, Italy
G. Abbiendi[a], A.C. Benvenuti[a], D. Bonacorsi[a,b], S. Braibant-Giacomelli[a,b], L. Brigliadori[a,b], R. Campanini[a,b], P. Capiluppi[a,b], A. Castro[a,b], F.R. Cavallo[a], G. Codispoti[a,b], M. Cuffiani[a,b], G.M. Dallavalle[a], F. Fabbri[a], A. Fanfani[a,b], D. Fasanella[a,b], P. Giacomelli[a], C. Grandi[a], L. Guiducci[a,b], S. Marcellini[a], G. Masetti[a], A. Montanari[a], F.L. Navarria[a,b], A. Perrotta[a], A.M. Rossi[a,b], T. Rovelli[a,b], G.P. Siroli[a,b], N. Tosi[a,b], R. Travaglini[a,b]

INFN Sezione di Catania [a], Università di Catania [b], CSFNSM [c], Catania, Italy
S. Albergo[a,b], G. Cappello[a], M. Chiorboli[a,b], S. Costa[a,b], F. Giordano[a,2], R. Potenza[a,b], A. Tricomi[a,b], C. Tuve[a,b]

INFN Sezione di Firenze [a], Università di Firenze [b], Firenze, Italy
G. Barbagli[a], V. Ciulli[a,b], C. Civinini[a], R. D'Alessandro[a,b], E. Focardi[a,b], E. Gallo[a], S. Gonzi[a,b], V. Gori[a,b], P. Lenzi[a,b], M. Meschini[a], S. Paoletti[a], G. Sguazzoni[a], A. Tropiano[a,b]

INFN Laboratori Nazionali di Frascati, Frascati, Italy
L. Benussi, S. Bianco, F. Fabbri, D. Piccolo

INFN Sezione di Genova [a], Università di Genova [b], Genova, Italy
R. Ferretti[a,b], F. Ferro[a], M. Lo Vetere[a,b], E. Robutti[a], S. Tosi[a,b]

INFN Sezione di Milano-Bicocca [a], Università di Milano-Bicocca [b], Milano, Italy
M.E. Dinardo[a,b], S. Fiorendi[a,b], S. Gennai[a,2], R. Gerosa[a,b,2], A. Ghezzi[a,b], P. Govoni[a,b], M.T. Lucchini[a,b,2], S. Malvezzi[a], R.A. Manzoni[a,b], A. Martelli[a,b], B. Marzocchi[a,b,2], D. Menasce[a], L. Moroni[a], M. Paganoni[a,b], D. Pedrini[a], S. Ragazzi[a,b], N. Redaelli[a], T. Tabarelli de Fatis[a,b]

INFN Sezione di Napoli [a]**, Università di Napoli 'Federico II'** [b]**, Università della Basilicata (Potenza)** [c]**, Università G. Marconi (Roma)** [d]**, Napoli, Italy**
S. Buontempo[a], N. Cavallo[a,c], S. Di Guida[a,d,2], F. Fabozzi[a,c], A.O.M. Iorio[a,b], L. Lista[a], S. Meola[a,d,2], M. Merola[a], P. Paolucci[a,2]

INFN Sezione di Padova [a]**, Università di Padova** [b]**, Università di Trento (Trento)** [c]**, Padova, Italy**
P. Azzi[a], N. Bacchetta[a], D. Bisello[a,b], A. Branca[a,b], R. Carlin[a,b], P. Checchia[a], M. Dall'Osso[a,b], T. Dorigo[a], U. Dosselli[a], F. Gasparini[a,b], U. Gasparini[a,b], A. Gozzelino[a], K. Kanishchev[a,c], S. Lacaprara[a], M. Margoni[a,b], A.T. Meneguzzo[a,b], J. Pazzini[a,b], N. Pozzobon[a,b], P. Ronchese[a,b], F. Simonetto[a,b], E. Torassa[a], M. Tosi[a,b], P. Zotto[a,b], A. Zucchetta[a,b], G. Zumerle[a,b]

INFN Sezione di Pavia [a]**, Università di Pavia** [b]**, Pavia, Italy**
M. Gabusi[a,b], S.P. Ratti[a,b], V. Re[a], C. Riccardi[a,b], P. Salvini[a], P. Vitulo[a,b]

INFN Sezione di Perugia [a]**, Università di Perugia** [b]**, Perugia, Italy**
M. Biasini[a,b], G.M. Bilei[a], D. Ciangottini[a,b,2], L. Fanò[a,b], P. Lariccia[a,b], G. Mantovani[a,b], M. Menichelli[a], A. Saha[a], A. Santocchia[a,b], A. Spiezia[a,b,2]

INFN Sezione di Pisa [a]**, Università di Pisa** [b]**, Scuola Normale Superiore di Pisa** [c]**, Pisa, Italy**
K. Androsov[a,26], P. Azzurri[a], G. Bagliesi[a], J. Bernardini[a], T. Boccali[a], G. Broccolo[a,c], R. Castaldi[a], M.A. Ciocci[a,26], R. Dell'Orso[a], S. Donato[a,c,2], G. Fedi, F. Fiori[a,c], L. Foà[a,c], A. Giassi[a], M.T. Grippo[a,26], F. Ligabue[a,c], T. Lomtadze[a], L. Martini[a,b], A. Messineo[a,b], C.S. Moon[a,27], F. Palla[a,2], A. Rizzi[a,b], A. Savoy-Navarro[a,28], A.T. Serban[a], P. Spagnolo[a], P. Squillacioti[a,26], R. Tenchini[a], G. Tonelli[a,b], A. Venturi[a], P.G. Verdini[a], C. Vernieri[a,c]

INFN Sezione di Roma [a]**, Università di Roma** [b]**, Roma, Italy**
L. Barone[a,b], F. Cavallari[a], G. D'imperio[a,b], D. Del Re[a,b], M. Diemoz[a], C. Jorda[a], E. Longo[a,b], F. Margaroli[a,b], P. Meridiani[a], F. Micheli[a,b,2], G. Organtini[a,b], R. Paramatti[a], S. Rahatlou[a,b], C. Rovelli[a], F. Santanastasio[a,b], L. Soffi[a,b], P. Traczyk[a,b,2]

INFN Sezione di Torino [a]**, Università di Torino** [b]**, Università del Piemonte Orientale (Novara)** [c]**, Torino, Italy**
N. Amapane[a,b], R. Arcidiacono[a,c], S. Argiro[a,b], M. Arneodo[a,c], R. Bellan[a,b], C. Biino[a], N. Cartiglia[a], S. Casasso[a,b,2], M. Costa[a,b], R. Covarelli, A. Degano[a,b], N. Demaria[a], L. Finco[a,b,2], C. Mariotti[a], S. Maselli[a], E. Migliore[a,b], V. Monaco[a,b], M. Musich[a], M.M. Obertino[a,c], L. Pacher[a,b], N. Pastrone[a], M. Pelliccioni[a], G.L. Pinna Angioni[a,b], A. Potenza[a,b], A. Romero[a,b], M. Ruspa[a,c], R. Sacchi[a,b], A. Solano[a,b], A. Staiano[a], U. Tamponi[a]

INFN Sezione di Trieste [a]**, Università di Trieste** [b]**, Trieste, Italy**
S. Belforte[a], V. Candelise[a,b,2], M. Casarsa[a], F. Cossutti[a], G. Della Ricca[a,b], B. Gobbo[a], C. La Licata[a,b], M. Marone[a,b], A. Schizzi[a,b], T. Umer[a,b], A. Zanetti[a]

Kangwon National University, Chunchon, Korea
S. Chang, A. Kropivnitskaya, S.K. Nam

Kyungpook National University, Daegu, Korea
D.H. Kim, G.N. Kim, M.S. Kim, D.J. Kong, S. Lee, Y.D. Oh, H. Park, A. Sakharov, D.C. Son

Chonbuk National University, Jeonju, Korea
T.J. Kim, M.S. Ryu

Chonnam National University, Institute for Universe and Elementary Particles, Kwangju, Korea
J.Y. Kim, D.H. Moon, S. Song

Korea University, Seoul, Korea
S. Choi, D. Gyun, B. Hong, M. Jo, H. Kim, Y. Kim, B. Lee, K.S. Lee, S.K. Park, Y. Roh

Seoul National University, Seoul, Korea
H.D. Yoo

University of Seoul, Seoul, Korea
M. Choi, J.H. Kim, I.C. Park, G. Ryu

Sungkyunkwan University, Suwon, Korea
Y. Choi, Y.K. Choi, J. Goh, D. Kim, E. Kwon, J. Lee, I. Yu

Vilnius University, Vilnius, Lithuania
A. Juodagalvis

National Centre for Particle Physics, Universiti Malaya, Kuala Lumpur, Malaysia
J.R. Komaragiri, M.A.B. Md Ali

Centro de Investigacion y de Estudios Avanzados del IPN, Mexico City, Mexico
E. Casimiro Linares, H. Castilla-Valdez, E. De La Cruz-Burelo, I. Heredia-de La Cruz, A. Hernandez-Almada, R. Lopez-Fernandez, A. Sanchez-Hernandez

Universidad Iberoamericana, Mexico City, Mexico
S. Carrillo Moreno, F. Vazquez Valencia

Benemerita Universidad Autonoma de Puebla, Puebla, Mexico
I. Pedraza, H.A. Salazar Ibarguen

Universidad Autónoma de San Luis Potosí, San Luis Potosí, Mexico
A. Morelos Pineda

University of Auckland, Auckland, New Zealand
D. Krofcheck

University of Canterbury, Christchurch, New Zealand
P.H. Butler, S. Reucroft

National Centre for Physics, Quaid-I-Azam University, Islamabad, Pakistan
A. Ahmad, M. Ahmad, Q. Hassan, H.R. Hoorani, W.A. Khan, T. Khurshid, M. Shoaib

National Centre for Nuclear Research, Swierk, Poland
H. Bialkowska, M. Bluj, B. Boimska, T. Frueboes, M. Górski, M. Kazana, K. Nawrocki, K. Romanowska-Rybinska, M. Szleper, P. Zalewski

Institute of Experimental Physics, Faculty of Physics, University of Warsaw, Warsaw, Poland
G. Brona, K. Bunkowski, M. Cwiok, W. Dominik, K. Doroba, A. Kalinowski, M. Konecki, J. Krolikowski, M. Misiura, M. Olszewski

Laboratório de Instrumentação e Física Experimental de Partículas, Lisboa, Portugal
P. Bargassa, C. Beirão Da Cruz E Silva, P. Faccioli, P.G. Ferreira Parracho, M. Gallinaro, L. Lloret Iglesias, F. Nguyen, J. Rodrigues Antunes, J. Seixas, J. Varela, P. Vischia

Joint Institute for Nuclear Research, Dubna, Russia
S. Afanasiev, P. Bunin, M. Gavrilenko, I. Golutvin, I. Gorbunov, A. Kamenev, V. Karjavin, V. Konoplyanikov, A. Lanev, A. Malakhov, V. Matveev[29], P. Moisenz, V. Palichik, V. Perelygin, S. Shmatov, N. Skatchkov, V. Smirnov, A. Zarubin

Petersburg Nuclear Physics Institute, Gatchina (St. Petersburg), Russia
V. Golovtsov, Y. Ivanov, V. Kim[30], E. Kuznetsova, P. Levchenko, V. Murzin, V. Oreshkin, I. Smirnov, V. Sulimov, L. Uvarov, S. Vavilov, A. Vorobyev, An. Vorobyev

Institute for Nuclear Research, Moscow, Russia
Yu. Andreev, A. Dermenev, S. Gninenko, N. Golubev, M. Kirsanov, N. Krasnikov, A. Pashenkov, D. Tlisov, A. Toropin

Institute for Theoretical and Experimental Physics, Moscow, Russia
V. Epshteyn, V. Gavrilov, N. Lychkovskaya, V. Popov, I. Pozdnyakov, G. Safronov, S. Semenov, A. Spiridonov, V. Stolin, E. Vlasov, A. Zhokin

P.N. Lebedev Physical Institute, Moscow, Russia
V. Andreev, M. Azarkin[31], I. Dremin[31], M. Kirakosyan, A. Leonidov[31], G. Mesyats, S.V. Rusakov, A. Vinogradov

Skobeltsyn Institute of Nuclear Physics, Lomonosov Moscow State University, Moscow, Russia
A. Belyaev, E. Boos, M. Dubinin[32], L. Dudko, A. Ershov, A. Gribushin, V. Klyukhin, O. Kodolova, I. Lokhtin, S. Obraztsov, S. Petrushanko, V. Savrin, A. Snigirev

State Research Center of Russian Federation, Institute for High Energy Physics, Protvino, Russia
I. Azhgirey, I. Bayshev, S. Bitioukov, V. Kachanov, A. Kalinin, D. Konstantinov, V. Krychkine, V. Petrov, R. Ryutin, A. Sobol, L. Tourtchanovitch, S. Troshin, N. Tyurin, A. Uzunian, A. Volkov

University of Belgrade, Faculty of Physics and Vinca Institute of Nuclear Sciences, Belgrade, Serbia
P. Adzic[33], M. Ekmedzic, J. Milosevic, V. Rekovic

Centro de Investigaciones Energéticas Medioambientales y Tecnológicas (CIEMAT), Madrid, Spain
J. Alcaraz Maestre, C. Battilana, E. Calvo, M. Cerrada, M. Chamizo Llatas, N. Colino, B. De La Cruz, A. Delgado Peris, D. Domínguez Vázquez, A. Escalante Del Valle, C. Fernandez Bedoya, J.P. Fernández Ramos, J. Flix, M.C. Fouz, P. Garcia-Abia, O. Gonzalez Lopez, S. Goy Lopez, J.M. Hernandez, M.I. Josa, E. Navarro De Martino, A. Pérez-Calero Yzquierdo, J. Puerta Pelayo, A. Quintario Olmeda, I. Redondo, L. Romero, M.S. Soares

Universidad Autónoma de Madrid, Madrid, Spain
C. Albajar, J.F. de Tróconiz, M. Missiroli, D. Moran

Universidad de Oviedo, Oviedo, Spain
H. Brun, J. Cuevas, J. Fernandez Menendez, S. Folgueras, I. Gonzalez Caballero

Instituto de Física de Cantabria (IFCA), CSIC-Universidad de Cantabria, Santander, Spain
J.A. Brochero Cifuentes, I.J. Cabrillo, A. Calderon, J. Duarte Campderros, M. Fernandez, G. Gomez, A. Graziano, A. Lopez Virto, J. Marco, R. Marco, C. Martinez Rivero, F. Matorras, F.J. Munoz Sanchez, J. Piedra Gomez, T. Rodrigo, A.Y. Rodríguez-Marrero, A. Ruiz-Jimeno, L. Scodellaro, I. Vila, R. Vilar Cortabitarte

CERN, European Organization for Nuclear Research, Geneva, Switzerland
D. Abbaneo, E. Auffray, G. Auzinger, M. Bachtis, P. Baillon, A.H. Ball, D. Barney, A. Benaglia, J. Bendavid, L. Benhabib, J.F. Benitez, P. Bloch, A. Bocci, A. Bonato, O. Bondu, C. Botta, H. Breuker, T. Camporesi, G. Cerminara, S. Colafranceschi[34], M. D'Alfonso, D. d'Enterria, A. Dabrowski, A. David, F. De Guio, A. De Roeck, S. De Visscher, E. Di Marco, M. Dobson,

M. Dordevic, B. Dorney, N. Dupont-Sagorin, A. Elliott-Peisert, G. Franzoni, W. Funk, D. Gigi, K. Gill, D. Giordano, M. Girone, F. Glege, R. Guida, S. Gundacker, M. Guthoff, J. Hammer, M. Hansen, P. Harris, J. Hegeman, V. Innocente, P. Janot, K. Kousouris, K. Krajczar, P. Lecoq, C. Lourenço, N. Magini, L. Malgeri, M. Mannelli, J. Marrouche, L. Masetti, F. Meijers, S. Mersi, E. Meschi, F. Moortgat, S. Morovic, M. Mulders, L. Orsini, L. Pape, E. Perez, A. Petrilli, G. Petrucciani, A. Pfeiffer, M. Pimiä, D. Piparo, M. Plagge, A. Racz, G. Rolandi[35], M. Rovere, H. Sakulin, C. Schäfer, C. Schwick, A. Sharma, P. Siegrist, P. Silva, M. Simon, P. Sphicas[36], D. Spiga, J. Steggemann, B. Stieger, M. Stoye, Y. Takahashi, D. Treille, A. Tsirou, G.I. Veres[18], N. Wardle, H.K. Wöhri, H. Wollny, W.D. Zeuner

Paul Scherrer Institut, Villigen, Switzerland
W. Bertl, K. Deiters, W. Erdmann, R. Horisberger, Q. Ingram, H.C. Kaestli, D. Kotlinski, U. Langenegger, D. Renker, T. Rohe

Institute for Particle Physics, ETH Zurich, Zurich, Switzerland
F. Bachmair, L. Bäni, L. Bianchini, M.A. Buchmann, B. Casal, N. Chanon, G. Dissertori, M. Dittmar, M. Donegà, M. Dünser, P. Eller, C. Grab, D. Hits, J. Hoss, W. Lustermann, B. Mangano, A.C. Marini, M. Marionneau, P. Martinez Ruiz del Arbol, M. Masciovecchio, D. Meister, N. Mohr, P. Musella, C. Nägeli[37], F. Nessi-Tedaldi, F. Pandolfi, F. Pauss, L. Perrozzi, M. Peruzzi, M. Quittnat, L. Rebane, M. Rossini, A. Starodumov[38], M. Takahashi, K. Theofilatos, R. Wallny, H.A. Weber

Universität Zürich, Zurich, Switzerland
C. Amsler[39], M.F. Canelli, V. Chiochia, A. De Cosa, A. Hinzmann, T. Hreus, B. Kilminster, C. Lange, J. Ngadiuba, D. Pinna, P. Robmann, F.J. Ronga, S. Taroni, M. Verzetti, Y. Yang

National Central University, Chung-Li, Taiwan
M. Cardaci, K.H. Chen, C. Ferro, C.M. Kuo, W. Lin, Y.J. Lu, R. Volpe, S.S. Yu

National Taiwan University (NTU), Taipei, Taiwan
P. Chang, Y.H. Chang, Y. Chao, K.F. Chen, P.H. Chen, C. Dietz, U. Grundler, W.-S. Hou, Y.F. Liu, R.-S. Lu, M. Miñano Moya, E. Petrakou, Y.M. Tzeng, R. Wilken

Chulalongkorn University, Faculty of Science, Department of Physics, Bangkok, Thailand
B. Asavapibhop, G. Singh, N. Srimanobhas, N. Suwonjandee

Cukurova University, Adana, Turkey
A. Adiguzel, M.N. Bakirci[40], S. Cerci[41], C. Dozen, I. Dumanoglu, E. Eskut, S. Girgis, G. Gokbulut, Y. Guler, E. Gurpinar, I. Hos, E.E. Kangal[42], A. Kayis Topaksu, G. Onengut[43], K. Ozdemir[44], S. Ozturk[40], A. Polatoz, D. Sunar Cerci[41], B. Tali[41], H. Topakli[40], M. Vergili, C. Zorbilmez

Middle East Technical University, Physics Department, Ankara, Turkey
I.V. Akin, B. Bilin, S. Bilmis, H. Gamsizkan[45], B. Isildak[46], G. Karapinar[47], K. Ocalan[48], S. Sekmen, U.E. Surat, M. Yalvac, M. Zeyrek

Bogazici University, Istanbul, Turkey
E.A. Albayrak[49], E. Gülmez, M. Kaya[50], O. Kaya[51], T. Yetkin[52]

Istanbul Technical University, Istanbul, Turkey
K. Cankocak, F.I. Vardarlı

National Scientific Center, Kharkov Institute of Physics and Technology, Kharkov, Ukraine
L. Levchuk, P. Sorokin

University of Bristol, Bristol, United Kingdom
J.J. Brooke, E. Clement, D. Cussans, H. Flacher, J. Goldstein, M. Grimes, G.P. Heath, H.F. Heath, J. Jacob, L. Kreczko, C. Lucas, Z. Meng, D.M. Newbold[53], S. Paramesvaran, A. Poll, T. Sakuma, S. Seif El Nasr-storey, S. Senkin, V.J. Smith

Rutherford Appleton Laboratory, Didcot, United Kingdom
K.W. Bell, A. Belyaev[54], C. Brew, R.M. Brown, D.J.A. Cockerill, J.A. Coughlan, K. Harder, S. Harper, E. Olaiya, D. Petyt, C.H. Shepherd-Themistocleous, A. Thea, I.R. Tomalin, T. Williams, W.J. Womersley, S.D. Worm

Imperial College, London, United Kingdom
M. Baber, R. Bainbridge, O. Buchmuller, D. Burton, D. Colling, N. Cripps, P. Dauncey, G. Davies, M. Della Negra, P. Dunne, A. Elwood, W. Ferguson, J. Fulcher, D. Futyan, G. Hall, G. Iles, M. Jarvis, G. Karapostoli, M. Kenzie, R. Lane, R. Lucas[53], L. Lyons, A.-M. Magnan, S. Malik, B. Mathias, J. Nash, A. Nikitenko[38], J. Pela, M. Pesaresi, K. Petridis, D.M. Raymond, S. Rogerson, A. Rose, C. Seez, P. Sharp[†], A. Tapper, M. Vazquez Acosta, T. Virdee, S.C. Zenz

Brunel University, Uxbridge, United Kingdom
J.E. Cole, P.R. Hobson, A. Khan, P. Kyberd, D. Leggat, D. Leslie, I.D. Reid, P. Symonds, L. Teodorescu, M. Turner

Baylor University, Waco, USA
J. Dittmann, K. Hatakeyama, A. Kasmi, H. Liu, N. Pastika, T. Scarborough, Z. Wu

The University of Alabama, Tuscaloosa, USA
O. Charaf, S.I. Cooper, C. Henderson, P. Rumerio

Boston University, Boston, USA
A. Avetisyan, T. Bose, C. Fantasia, P. Lawson, C. Richardson, J. Rohlf, J. St. John, L. Sulak

Brown University, Providence, USA
J. Alimena, E. Berry, S. Bhattacharya, G. Christopher, D. Cutts, Z. Demiragli, N. Dhingra, A. Ferapontov, A. Garabedian, U. Heintz, G. Kukartsev, E. Laird, G. Landsberg, M. Luk, M. Narain, M. Segala, T. Sinthuprasith, T. Speer, J. Swanson

University of California, Davis, Davis, USA
R. Breedon, G. Breto, M. Calderon De La Barca Sanchez, S. Chauhan, M. Chertok, J. Conway, R. Conway, P.T. Cox, R. Erbacher, M. Gardner, W. Ko, R. Lander, M. Mulhearn, D. Pellett, J. Pilot, F. Ricci-Tam, S. Shalhout, J. Smith, M. Squires, D. Stolp, M. Tripathi, S. Wilbur, R. Yohay

University of California, Los Angeles, USA
R. Cousins, P. Everaerts, C. Farrell, J. Hauser, M. Ignatenko, G. Rakness, E. Takasugi, V. Valuev, M. Weber

University of California, Riverside, Riverside, USA
K. Burt, R. Clare, J. Ellison, J.W. Gary, G. Hanson, J. Heilman, M. Ivova Rikova, P. Jandir, E. Kennedy, F. Lacroix, O.R. Long, A. Luthra, M. Malberti, M. Olmedo Negrete, A. Shrinivas, S. Sumowidagdo, S. Wimpenny

University of California, San Diego, La Jolla, USA
J.G. Branson, G.B. Cerati, S. Cittolin, R.T. D'Agnolo, A. Holzner, R. Kelley, D. Klein, J. Letts, I. Macneill, D. Olivito, S. Padhi, C. Palmer, M. Pieri, M. Sani, V. Sharma, S. Simon, M. Tadel, Y. Tu, A. Vartak, C. Welke, F. Würthwein, A. Yagil, G. Zevi Della Porta

University of California, Santa Barbara, Santa Barbara, USA
D. Barge, J. Bradmiller-Feld, C. Campagnari, T. Danielson, A. Dishaw, V. Dutta, K. Flowers, M. Franco Sevilla, P. Geffert, C. George, F. Golf, L. Gouskos, J. Incandela, C. Justus, N. Mccoll, S.D. Mullin, J. Richman, D. Stuart, W. To, C. West, J. Yoo

California Institute of Technology, Pasadena, USA
A. Apresyan, A. Bornheim, J. Bunn, Y. Chen, J. Duarte, A. Mott, H.B. Newman, C. Pena, M. Pierini, M. Spiropulu, J.R. Vlimant, R. Wilkinson, S. Xie, R.Y. Zhu

Carnegie Mellon University, Pittsburgh, USA
V. Azzolini, A. Calamba, B. Carlson, T. Ferguson, Y. Iiyama, M. Paulini, J. Russ, H. Vogel, I. Vorobiev

University of Colorado at Boulder, Boulder, USA
J.P. Cumalat, W.T. Ford, A. Gaz, M. Krohn, E. Luiggi Lopez, U. Nauenberg, J.G. Smith, K. Stenson, S.R. Wagner

Cornell University, Ithaca, USA
J. Alexander, A. Chatterjee, J. Chaves, J. Chu, S. Dittmer, N. Eggert, N. Mirman, G. Nicolas Kaufman, J.R. Patterson, A. Ryd, E. Salvati, L. Skinnari, W. Sun, W.D. Teo, J. Thom, J. Thompson, J. Tucker, Y. Weng, L. Winstrom, P. Wittich

Fairfield University, Fairfield, USA
D. Winn

Fermi National Accelerator Laboratory, Batavia, USA
S. Abdullin, M. Albrow, J. Anderson, G. Apollinari, L.A.T. Bauerdick, A. Beretvas, J. Berryhill, P.C. Bhat, G. Bolla, K. Burkett, J.N. Butler, H.W.K. Cheung, F. Chlebana, S. Cihangir, V.D. Elvira, I. Fisk, J. Freeman, E. Gottschalk, L. Gray, D. Green, S. Grünendahl, O. Gutsche, J. Hanlon, D. Hare, R.M. Harris, J. Hirschauer, B. Hooberman, S. Jindariani, M. Johnson, U. Joshi, B. Klima, B. Kreis, S. Kwan[†], J. Linacre, D. Lincoln, R. Lipton, T. Liu, J. Lykken, K. Maeshima, J.M. Marraffino, V.I. Martinez Outschoorn, S. Maruyama, D. Mason, P. McBride, P. Merkel, K. Mishra, S. Mrenna, S. Nahn, C. Newman-Holmes, V. O'Dell, O. Prokofyev, E. Sexton-Kennedy, A. Soha, W.J. Spalding, L. Spiegel, L. Taylor, S. Tkaczyk, N.V. Tran, L. Uplegger, E.W. Vaandering, R. Vidal, A. Whitbeck, J. Whitmore, F. Yang

University of Florida, Gainesville, USA
D. Acosta, P. Avery, P. Bortignon, D. Bourilkov, M. Carver, D. Curry, S. Das, M. De Gruttola, G.P. Di Giovanni, R.D. Field, M. Fisher, I.K. Furic, J. Hugon, J. Konigsberg, A. Korytov, T. Kypreos, J.F. Low, K. Matchev, H. Mei, P. Milenovic[55], G. Mitselmakher, L. Muniz, A. Rinkevicius, L. Shchutska, M. Snowball, D. Sperka, J. Yelton, M. Zakaria

Florida International University, Miami, USA
S. Hewamanage, S. Linn, P. Markowitz, G. Martinez, J.L. Rodriguez

Florida State University, Tallahassee, USA
J.R. Adams, T. Adams, A. Askew, J. Bochenek, B. Diamond, J. Haas, S. Hagopian, V. Hagopian, K.F. Johnson, H. Prosper, V. Veeraraghavan, M. Weinberg

Florida Institute of Technology, Melbourne, USA
M.M. Baarmand, M. Hohlmann, H. Kalakhety, F. Yumiceva

University of Illinois at Chicago (UIC), Chicago, USA
M.R. Adams, L. Apanasevich, D. Berry, R.R. Betts, I. Bucinskaite, R. Cavanaugh, O. Evdokimov,

L. Gauthier, C.E. Gerber, D.J. Hofman, P. Kurt, C. O'Brien, I.D. Sandoval Gonzalez, C. Silkworth, P. Turner, N. Varelas

The University of Iowa, Iowa City, USA
B. Bilki[56], W. Clarida, K. Dilsiz, M. Haytmyradov, J.-P. Merlo, H. Mermerkaya[57], A. Mestvirishvili, A. Moeller, J. Nachtman, H. Ogul, Y. Onel, F. Ozok[49], A. Penzo, R. Rahmat, S. Sen, P. Tan, E. Tiras, J. Wetzel, K. Yi

Johns Hopkins University, Baltimore, USA
I. Anderson, B.A. Barnett, B. Blumenfeld, S. Bolognesi, D. Fehling, A.V. Gritsan, P. Maksimovic, C. Martin, M. Swartz, M. Xiao

The University of Kansas, Lawrence, USA
P. Baringer, A. Bean, G. Benelli, C. Bruner, J. Gray, R.P. Kenny III, D. Majumder, M. Malek, M. Murray, D. Noonan, S. Sanders, J. Sekaric, R. Stringer, Q. Wang, J.S. Wood

Kansas State University, Manhattan, USA
I. Chakaberia, A. Ivanov, K. Kaadze, S. Khalil, M. Makouski, Y. Maravin, L.K. Saini, N. Skhirtladze, I. Svintradze

Lawrence Livermore National Laboratory, Livermore, USA
J. Gronberg, D. Lange, F. Rebassoo, D. Wright

University of Maryland, College Park, USA
A. Baden, A. Belloni, B. Calvert, S.C. Eno, J.A. Gomez, N.J. Hadley, S. Jabeen, R.G. Kellogg, T. Kolberg, Y. Lu, A.C. Mignerey, K. Pedro, A. Skuja, M.B. Tonjes, S.C. Tonwar

Massachusetts Institute of Technology, Cambridge, USA
A. Apyan, R. Barbieri, K. Bierwagen, W. Busza, I.A. Cali, L. Di Matteo, G. Gomez Ceballos, M. Goncharov, D. Gulhan, M. Klute, Y.S. Lai, Y.-J. Lee, A. Levin, P.D. Luckey, C. Paus, D. Ralph, C. Roland, G. Roland, G.S.F. Stephans, K. Sumorok, D. Velicanu, J. Veverka, B. Wyslouch, M. Yang, M. Zanetti, V. Zhukova

University of Minnesota, Minneapolis, USA
B. Dahmes, A. Gude, S.C. Kao, K. Klapoetke, Y. Kubota, J. Mans, S. Nourbakhsh, R. Rusack, A. Singovsky, N. Tambe, J. Turkewitz

University of Mississippi, Oxford, USA
J.G. Acosta, S. Oliveros

University of Nebraska-Lincoln, Lincoln, USA
E. Avdeeva, K. Bloom, S. Bose, D.R. Claes, A. Dominguez, R. Gonzalez Suarez, J. Keller, D. Knowlton, I. Kravchenko, J. Lazo-Flores, F. Meier, F. Ratnikov, G.R. Snow, M. Zvada

State University of New York at Buffalo, Buffalo, USA
J. Dolen, A. Godshalk, I. Iashvili, A. Kharchilava, A. Kumar, S. Rappoccio

Northeastern University, Boston, USA
G. Alverson, E. Barberis, D. Baumgartel, M. Chasco, A. Massironi, D.M. Morse, D. Nash, T. Orimoto, D. Trocino, R.-J. Wang, D. Wood, J. Zhang

Northwestern University, Evanston, USA
K.A. Hahn, A. Kubik, N. Mucia, N. Odell, B. Pollack, A. Pozdnyakov, M. Schmitt, S. Stoynev, K. Sung, M. Velasco, S. Won

University of Notre Dame, Notre Dame, USA
A. Brinkerhoff, K.M. Chan, A. Drozdetskiy, M. Hildreth, C. Jessop, D.J. Karmgard, N. Kellams, K. Lannon, S. Lynch, N. Marinelli, Y. Musienko[29], T. Pearson, M. Planer, R. Ruchti, G. Smith, N. Valls, M. Wayne, M. Wolf, A. Woodard

The Ohio State University, Columbus, USA
L. Antonelli, J. Brinson, B. Bylsma, L.S. Durkin, S. Flowers, A. Hart, C. Hill, R. Hughes, K. Kotov, T.Y. Ling, W. Luo, D. Puigh, M. Rodenburg, B.L. Winer, H. Wolfe, H.W. Wulsin

Princeton University, Princeton, USA
O. Driga, P. Elmer, J. Hardenbrook, P. Hebda, S.A. Koay, P. Lujan, D. Marlow, T. Medvedeva, M. Mooney, J. Olsen, P. Piroué, X. Quan, H. Saka, D. Stickland[2], C. Tully, J.S. Werner, A. Zuranski

University of Puerto Rico, Mayaguez, USA
E. Brownson, S. Malik, H. Mendez, J.E. Ramirez Vargas

Purdue University, West Lafayette, USA
V.E. Barnes, D. Benedetti, D. Bortoletto, M. De Mattia, L. Gutay, Z. Hu, M.K. Jha, M. Jones, K. Jung, M. Kress, N. Leonardo, D.H. Miller, N. Neumeister, F. Primavera, B.C. Radburn-Smith, X. Shi, I. Shipsey, D. Silvers, A. Svyatkovskiy, F. Wang, W. Xie, L. Xu, J. Zablocki

Purdue University Calumet, Hammond, USA
N. Parashar, J. Stupak

Rice University, Houston, USA
A. Adair, B. Akgun, K.M. Ecklund, F.J.M. Geurts, W. Li, B. Michlin, B.P. Padley, R. Redjimi, J. Roberts, J. Zabel

University of Rochester, Rochester, USA
B. Betchart, A. Bodek, P. de Barbaro, R. Demina, Y. Eshaq, T. Ferbel, M. Galanti, A. Garcia-Bellido, P. Goldenzweig, J. Han, A. Harel, O. Hindrichs, A. Khukhunaishvili, S. Korjenevski, G. Petrillo, D. Vishnevskiy

The Rockefeller University, New York, USA
R. Ciesielski, L. Demortier, K. Goulianos, C. Mesropian

Rutgers, The State University of New Jersey, Piscataway, USA
S. Arora, A. Barker, J.P. Chou, C. Contreras-Campana, E. Contreras-Campana, D. Duggan, D. Ferencek, Y. Gershtein, R. Gray, E. Halkiadakis, D. Hidas, S. Kaplan, A. Lath, S. Panwalkar, M. Park, R. Patel, S. Salur, S. Schnetzer, D. Sheffield, S. Somalwar, R. Stone, S. Thomas, P. Thomassen, M. Walker

University of Tennessee, Knoxville, USA
K. Rose, S. Spanier, A. York

Texas A&M University, College Station, USA
O. Bouhali[58], A. Castaneda Hernandez, R. Eusebi, W. Flanagan, J. Gilmore, T. Kamon[59], V. Khotilovich, V. Krutelyov, R. Montalvo, I. Osipenkov, Y. Pakhotin, A. Perloff, J. Roe, A. Rose, A. Safonov, I. Suarez, A. Tatarinov, K.A. Ulmer

Texas Tech University, Lubbock, USA
N. Akchurin, C. Cowden, J. Damgov, C. Dragoiu, P.R. Dudero, J. Faulkner, K. Kovitanggoon, S. Kunori, S.W. Lee, T. Libeiro, I. Volobouev

Vanderbilt University, Nashville, USA
E. Appelt, A.G. Delannoy, S. Greene, A. Gurrola, W. Johns, C. Maguire, Y. Mao, A. Melo, M. Sharma, P. Sheldon, B. Snook, S. Tuo, J. Velkovska

University of Virginia, Charlottesville, USA
M.W. Arenton, S. Boutle, B. Cox, B. Francis, J. Goodell, R. Hirosky, A. Ledovskoy, H. Li, C. Lin, C. Neu, E. Wolfe, J. Wood

Wayne State University, Detroit, USA
C. Clarke, R. Harr, P.E. Karchin, C. Kottachchi Kankanamge Don, P. Lamichhane, J. Sturdy

University of Wisconsin, Madison, USA
D.A. Belknap, D. Carlsmith, M. Cepeda, S. Dasu, L. Dodd, S. Duric, E. Friis, R. Hall-Wilton, M. Herndon, A. Hervé, P. Klabbers, A. Lanaro, C. Lazaridis, A. Levine, R. Loveless, A. Mohapatra, I. Ojalvo, T. Perry, G.A. Pierro, G. Polese, I. Ross, T. Sarangi, A. Savin, W.H. Smith, D. Taylor, C. Vuosalo, N. Woods

†: Deceased
1: Also at Vienna University of Technology, Vienna, Austria
2: Also at CERN, European Organization for Nuclear Research, Geneva, Switzerland
3: Also at Institut Pluridisciplinaire Hubert Curien, Université de Strasbourg, Université de Haute Alsace Mulhouse, CNRS/IN2P3, Strasbourg, France
4: Also at National Institute of Chemical Physics and Biophysics, Tallinn, Estonia
5: Also at Skobeltsyn Institute of Nuclear Physics, Lomonosov Moscow State University, Moscow, Russia
6: Also at Universidade Estadual de Campinas, Campinas, Brazil
7: Also at Laboratoire Leprince-Ringuet, Ecole Polytechnique, IN2P3-CNRS, Palaiseau, France
8: Also at Joint Institute for Nuclear Research, Dubna, Russia
9: Also at Suez University, Suez, Egypt
10: Also at Cairo University, Cairo, Egypt
11: Also at Fayoum University, El-Fayoum, Egypt
12: Also at British University in Egypt, Cairo, Egypt
13: Now at Sultan Qaboos University, Muscat, Oman
14: Also at Université de Haute Alsace, Mulhouse, France
15: Also at Ilia State University, Tbilisi, Georgia
16: Also at Brandenburg University of Technology, Cottbus, Germany
17: Also at Institute of Nuclear Research ATOMKI, Debrecen, Hungary
18: Also at Eötvös Loránd University, Budapest, Hungary
19: Also at University of Debrecen, Debrecen, Hungary
20: Also at University of Visva-Bharati, Santiniketan, India
21: Now at King Abdulaziz University, Jeddah, Saudi Arabia
22: Also at University of Ruhuna, Matara, Sri Lanka
23: Also at Isfahan University of Technology, Isfahan, Iran
24: Also at University of Tehran, Department of Engineering Science, Tehran, Iran
25: Also at Plasma Physics Research Center, Science and Research Branch, Islamic Azad University, Tehran, Iran
26: Also at Università degli Studi di Siena, Siena, Italy
27: Also at Centre National de la Recherche Scientifique (CNRS) - IN2P3, Paris, France
28: Also at Purdue University, West Lafayette, USA
29: Also at Institute for Nuclear Research, Moscow, Russia
30: Also at St. Petersburg State Polytechnical University, St. Petersburg, Russia

31: Also at National Research Nuclear University "Moscow Engineering Physics Institute" (MEPhI), Moscow, Russia
32: Also at California Institute of Technology, Pasadena, USA
33: Also at Faculty of Physics, University of Belgrade, Belgrade, Serbia
34: Also at Facoltà Ingegneria, Università di Roma, Roma, Italy
35: Also at Scuola Normale e Sezione dell'INFN, Pisa, Italy
36: Also at University of Athens, Athens, Greece
37: Also at Paul Scherrer Institut, Villigen, Switzerland
38: Also at Institute for Theoretical and Experimental Physics, Moscow, Russia
39: Also at Albert Einstein Center for Fundamental Physics, Bern, Switzerland
40: Also at Gaziosmanpasa University, Tokat, Turkey
41: Also at Adiyaman University, Adiyaman, Turkey
42: Also at Mersin University, Mersin, Turkey
43: Also at Cag University, Mersin, Turkey
44: Also at Piri Reis University, Istanbul, Turkey
45: Also at Anadolu University, Eskisehir, Turkey
46: Also at Ozyegin University, Istanbul, Turkey
47: Also at Izmir Institute of Technology, Izmir, Turkey
48: Also at Necmettin Erbakan University, Konya, Turkey
49: Also at Mimar Sinan University, Istanbul, Istanbul, Turkey
50: Also at Marmara University, Istanbul, Turkey
51: Also at Kafkas University, Kars, Turkey
52: Also at Yildiz Technical University, Istanbul, Turkey
53: Also at Rutherford Appleton Laboratory, Didcot, United Kingdom
54: Also at School of Physics and Astronomy, University of Southampton, Southampton, United Kingdom
55: Also at University of Belgrade, Faculty of Physics and Vinca Institute of Nuclear Sciences, Belgrade, Serbia
56: Also at Argonne National Laboratory, Argonne, USA
57: Also at Erzincan University, Erzincan, Turkey
58: Also at Texas A&M University at Qatar, Doha, Qatar
59: Also at Kyungpook National University, Daegu, Korea